The Pennsylvania State University

The Graduate School

The Eberly College of Science

DRIVING THERMALLY-ACTIVATED CHEMICAL REACTIONS WITH MOLECULAR-SCALE CONTROL USING THE PHOTOTHERMAL EFFECT OF NANOPARTICLES

A Dissertation in

Chemistry

by

Kaitlin Haas

Submitted in Partial Fulfillment
of the Requirements
for the Degree of

Doctor of Philosophy

August 2015

The dissertation of Kaitlin Haas was reviewed and approved* by the following:

Benjamin Lear
Assistant Professor of Chemistry
Dissertation Advisor
Chair of Committee

Christine Dolan Keating
Professor of Chemistry

Tom Mallouk
Evan Pugh Professor of Chemistry, Physics, Biochemistry and Molecular Biology
Head of the Chemistry Department

Chris Giebink
Assistant Professor of Electrical Engineering

*Signatures are on file in the Graduate School

ABSTRACT

Photoexcitation of the surface plasmon in gold nanoparticles (AuNPs) results in the production of high temperatures at the nanoparticle surface in what is referred to as the photothermal effect. The heat from this phenomenon is rapidly generated (~10 ps) and is highly localized (< 20 nm), providing high resolution temporal and spatial control over a molecular-scale heat source. Thus far, this heat has been utilized to ablate cancer cells, run high temperature reactions, and decompose polymers. However, little is known about the constructive power and the temperatures achieved by this effect, and more importantly, the properties that influence our control over this heat. The work in this dissertation demonstrates the general applicability of photothermal heat to various chemical transformations, such as bond formation, and utilizes kinetic data to estimate photothermal temperatures. We also investigate other materials as potential photothermal agents. Collectively, this work provides a better understanding of the photothermal effect, and establishes it as a well-controlled and on-demand heat source.

TABLE OF CONTENTS

LIST OF FIGURES

LIST OF SCHEMES

LIST OF TABLES

ACKNOWLEDGEMENTS

To my family: Thank you for instilling in me the value of hard work, and the understanding that while reaching your goals isn't easy, it is well worth the effort. Your love, support, and patience (and food and money) continue to make me a better person

To my friends: Thank you for the phone calls, care packages, visits, conversations, and laughter. Making science is serious business, and your reminders to laugh (and beer) were the lifeline to my sanity.

To the Lear Lab: Thank you for making me a better scientist, communicator, and student. The greatest learning experiences I have had during grad school have been because of you, and I continue to learn from all of you. Make good science, and continue to keep your minds open.

While I cannot find the words to properly express my gratitude to all those that have helped shape me on my journey, please know that I would not be where I am today without you. I will continue to learn from you, and more importantly, share what I have learned with others.

Chapter 1

Driving Chemical Reactions via Photothermal Heating

Heat as a Synthetic Tool

Improvements in synthetic techniques have often formed the foundation of ground breaking discoveries and advances across all fields of science and technology. Electron-beam lithography photolithography enabled high resolution patterning at the nanometer scale used in the fabrication of computer processors capable of speeds nearly ten thousand times faster than those 30 years ago.[1] Reactive ion etching allowed the miniaturization of surgical needles that deliver medicine with both increased control and precise dosage.[2] Synthetic modification of specific genes through DNA editing, previously only accomplished by nature, provides the ability to create, delete, activate, and suppress targeted genes in various organisms.[3] In all of these cases, it is evident that greater control over the manufacture of materials and chemicals has played a large role in scientific advancements. It is paramount that we continue to develop new synthetic methods in order to facilitate future advances.

In the history of synthetic techniques, heat may be the oldest and most fundamental tool for driving molecular transformations: the formation, breaking, and isomerization of chemical bonds. As such, heat is widely used in many disciplines such as material science, medicine, agriculture, and electronics and lies at the foundation of our modern lifestyle. For instance, the Haber-Bosch process, which is conducted at temperatures in excess of 400°C, produces ammonia for fertilizer, and is estimated to be responsible for sustaining one-third of the Earth's population.[4] Thermal cracking of hydrocarbons is another high temperature process that is essential to the field of petroleum chemistry, and produces much needed substances such as ethylene and petroleum

coke.[5] The retro Diels-Alder reaction is a versatile low temperature (~60°C) reaction employed in drug delivery and self-healing polymers.[5-9] Thus, heat remains a versatile and important tool in modern science and technology.

The general utility of heat stems from the fact that every molecular transformation has an energy barrier that must be overcome in order to generate a product. At a given temperature, the random thermal motion of atoms can occasionally provide sufficient energy to overcome this energy barrier; however, the probability that a molecule will have enough energy is exponentially dependent on temperature. There are two ways in which the barrier is addressed: increasing the temperature or decreasing the barrier (catalyst). Providing additional thermal energy through heat transfer can greatly increase the fraction of molecules with sufficient energy to overcome the energy barrier and form products. As heat is added to a sample and the temperature increased, the fraction of total collisions with enough energy and proper orientation to overcome the energy barrier and form products increases, as shown in the Arrhenius equation below.

$$k = Ae^{-E_a/(RT)} \qquad (1\text{-}1)$$

where A represents the fraction of collisions and $-E_a/RT$ represent the likelihood of these collisions to overcome the barrier. As a tool, heat can be broadly applied to a wide variety of reactions, but it can also result in undesired side reactions. Catalysts, which are often used to increase rates of reactions, can also be used to induce high stereospecificity under mild conditions and reduce side reactions. However, catalysts are often effective for very specific substrates which means they need to be developed on a reaction-by-reaction basis, can be expensive (many catalysts utilize palladium, rhodium, or iridium), and are often difficult to recover if they are homogenous.[10]

In addition to kinetic considerations, reactions at thermodynamic equilibrium can be affected by variables such as pressure, concentration, and temperature. Other reactions rely on specific formulations to create products with particular properties that would be altered by changes in reactant concentration and pressure. For instance, the rigidity and flexibility of a

polymer can be tuned by altering the concentration of its starting materials. Thus, to overcome these obstacles, heat can be utilized to drive a reaction towards the products without altering the composition.

Problems with Heat

While the above makes it evident that heat is widely applicable to numerous valuable processes, the general utility of heat is offset by its wild inefficiency. This inefficiency arises primarily from two problems. The first problem is loss of heat to the surroundings through thermal radiation and convection. Thus, energy must be continually added in order to maintain constant temperature. The second problem results from a fundamental mismatch between the scale of heat application and the system undergoing transformation – a problem that is particularly acute for many chemical transformations where heat is often applied on the meter scale in order to accomplish transitions on the nanometer scale. Additionally, the reactive molecules compose only a small fraction of the entire material. For example, a 1 M solution of reactant in water will have a mole fraction of solute that is < 2%, yet heat is must be supplied to the entire solution in order to effect changes on this minor component.

The degree of these inefficiencies can be highlighted by considering a common industrial application of heat: the curing of polymer films, such as those on vehicles or machinery. The current state-of-the-art for curing these films on automotive bodies is to: (i) assemble the frame of the car, (ii) apply the coating to the surface of the car, and (iii) pass the coated car and frame through an open oven on a conveyer belt. The losses due to both thermal radiation and convection are quite large, given the open nature of these ovens. The problem of mismatch between the size of the reactive system (film) and the total scale of heat being applied (the full frame of the car) is easily illustrated. A car of average size will have a film that has a mass that is ~0.10% that of the car's; considering the heat capacity of the frame and film, conventional

heating methods provide nearly 400 times the amount of energy that is absolutely necessary to cure the film, and thus 0.25% efficient. Furthermore, this estimated inefficiency does not account for unintended thermal absorbers, such as the oven or other materials present, the time consumed to heat these structures, or heat lost through the open oven. Thus, while this heating method is effective at curing films, the energy consumed during the process increases the energy and financial cost beyond what is strictly needed. If we increased the precision of heat application, we could increase its efficiency.

Though the above is an example of thermal inefficiencies on a grand scale, there are similar problems with all bulk-scale applications of heat. To a large extent, this is a result of cultural inertia. Many of the heating techniques utilized today were developed decades ago, and do prove effective. For example, microwave heating is a heating technique can directly access rotational and vibrational modes of molecules and potentially heat a system within a matter of seconds - a rate significantly faster than heating via ovens.[11] However, like ovens, this technique provides bulk-scale heating, which results in excessive energy costs, and the increasing awareness of the need to conserve energy makes these approaches inadequate for the needs of present day. There is also an additional difficulty in addressing the problem of scale mismatch – until the advent of synthetic nanoscience, it was difficult to envision a way to apply heat with a level of control that approached the molecular scale. Gaining such control over the application of heat will certainly overcome many of the inefficiencies associated with thermal reactions, such as avoidance of unwanted reactivity. It will also enable new applications. For instance, driving high temperature reactions (i.e. urethane polymerization) on substrates that are thermally sensitive (i.e. skin). Therefore, a large opportunity presents itself for the development of a new heating method that will apply heat in a more efficient and controlled manner. The demonstration of such a method is the goal of this dissertation.

Successful completion of this overall goal requires identification of a heat source that can provide precise spatial and temporal control over heat sufficient to drive a reaction. For this

dissertation, we use the photothermal effect exhibited by plasmonic metallic nanoparticles as this heat source. Below, we demonstrate how gold nanoparticles meet our demands.

The Plasmon of Metallic Nanoparticles

Metal nanoparticles, such as gold (AuNPs), possess a surface plasmon which is an electromagnetic wave composed of conduction electrons that propagates along the surface of a metal surface. Upon application of an electric field, such as light, a polarization of these free electrons with respect to the much heavier metallic core occurs (Figure **1-1**).[12] Coulombic attraction between the displaced electron cloud and the positive metal core acts as a restorative force, producing a coherent dipolar oscillation at the particle's surface.[13] The natural frequency of this resonance is dependent on the size, shape, and identity of the metal.[14] Shining light with a frequency that matches the natural frequency of the surface plasmon's oscillations results in resonant driving of the electrons, producing a large enhancement in the near-field amplitude of plasmon's electric field that can in turn enhance the interaction of light (absorption and scattering) with the metal.[15,16]

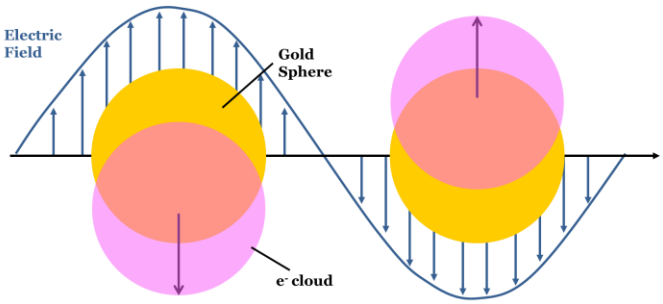

Figure **1-1**: The production of a surface plasmon at the nanoparticle surface.

Because of the strong interaction with light, the surface plasmon resonance (SPR) leads to a strong extinction band in the UV-Vis spectrum for AuNPs, and is responsible for the brightly

colored appearance of colloidal solutions of metal nanoparticles.[17] As noted above, the position of this feature is sensitive to the physical properties of the nanoparticle (e.g. size, shape, material) (Figure **1-2**). However, it is also sensitive to the medium – specifically, the dielectric constant.[18] This sensitivity provides the ability to detect changes in the immediate environment of the nanoparticle, and has been exploited in areas such as molecular adsorption and microscopy.[19,20] While both scattering and absorption contribute to the total extinction of the particle, it is the absorption of light that ultimately results in heat production. Therefore, in order to maximize heat production, it is important to understand how to control the interaction of nanoparticles with light, which can be mathematically described by Mie theory.[21]

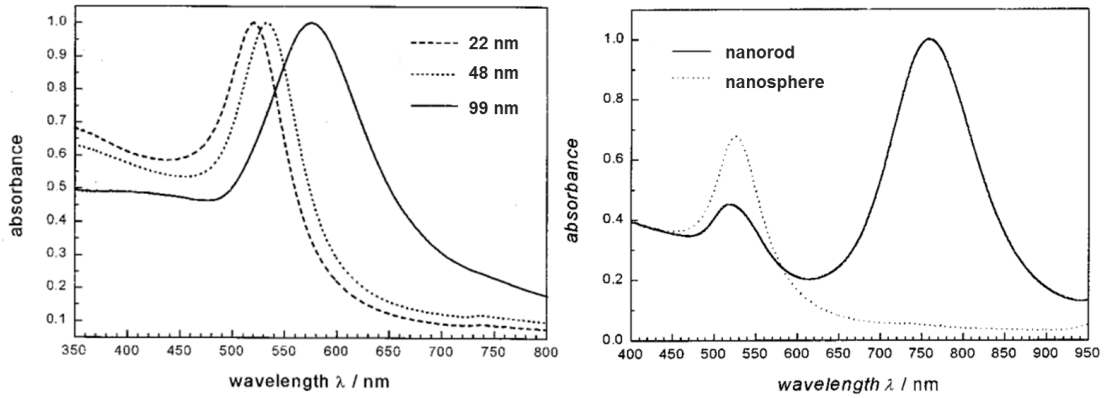

Figure **1-2**: UV-Vis spectra of various gold nanoparticles, showing how a) size and b) shape of gold nanoparticles affect the SPR.[12,22]

Determining the Absorptivity of Metallic Particles Using Mie Theory

The basic physics governing the interaction of electromagnetic fields of light with plasmons was first described by Gustav Mie in 1908 for spherical particles much smaller than the wavelength of incident light ($2r << \lambda_{max}/10$) .[12] Mie theory can be used to precisely calculate the spectra of spherical particles, and is an exact solution to Maxwell's equations for spheres with an arbitrary size.[23] Mie's solution to Maxwell's equations describes the optical response of

spherical particle to light, and can be used to calculate a nanoparticle's extinction cross section (σ), a geometrical quantity which relates incident light to the scattering and absorption power of the particle. The extinction cross section (σ_{ext}) is simply the sum of the scattering (σ_{ext}) and absorption (σ_{abs}) cross sections[12,23]

$$\sigma_{ext} = \sigma_{sca} + \sigma_{abs} \tag{1-2}$$

which can be expressed by

$$\sigma_{ext} = \frac{2\pi r^2}{x^2}\sum_{n=1}^{\infty}(2n+1)Re(a_n + b_n) \tag{1-3}$$

$$\sigma_{sca} = \frac{2\pi r^2}{x^2}\sum_{n=1}^{\infty}(2n+1)(|a_n|^2 + |b_n|^2) \tag{1-4}$$

$$\sigma_{abs} = \frac{18\pi V}{\lambda}\varepsilon_m^{3/2}\frac{\varepsilon_2}{(\varepsilon_1 + 2\varepsilon_m)^2 + \varepsilon_2^2} \tag{1-5}$$

and the Mie coefficients

$$a_n = \frac{\psi_n'(mx)\psi_n(x) - m\psi_n(mx)\psi_n'(x)}{\psi_n'(mx)\zeta_n(x) - m\psi_n(mx)\zeta_n'x} \tag{1-6}$$

$$b_n = \frac{m\psi_n'(mx)\psi_n(x) - \psi_n(mx)\psi_n'(x)}{m\psi_n'(mx)\zeta_n(x) - \psi_n(mx)\zeta_n'(x)} \tag{1-7}$$

where x is the size parameter given by $2\pi R n_m/\lambda$, r is the nanoparticle radius, n_m is the refractive index of the medium, and V is the volume of the particle.[23] ε_m and $\varepsilon = \varepsilon_1 + i\varepsilon_2$ are the dielectric functions of the surrounding medium and material respectively, and ε_1 and ε_2 represent the real and imaginary parts of the dielectric function of the material (ε). The ratio of the complex refractive indices of the particle and surrounding medium is $m = n/n_m$, ψ_n and ζ_n are the Riccati-Bessel cylindrical functions that account for how charged particles scatter from each other, and a prime indicates that the differentiation is applied to the argument in parentheses.[24]

When nanoparticles are significantly smaller than the wavelength of incident light ($2r < \lambda_{max}/10$), the extinction coefficient only receives significant contributions from the dipole oscillation, and equation **1-3** can be reduced to

$$\sigma_{ext} = \frac{9\omega V}{c}\varepsilon_m^{3/2}\frac{\varepsilon_2}{(\varepsilon_1 + 2\varepsilon_m)^2 + \varepsilon_2^2} \quad (1\text{-}8)$$

where V is the particle's volume, ω is the angular frequency of the incident light, c is the speed of light, and ε_m is the dielectric function of the surrounding medium.[12,25]

These equations show that the properties of the SPR are highly dependent on nanoparticle dimensions. For example, the contributions of the scattering and absorption coefficients to the total particle's extinction cross section can be calculated for different sized particles. By dividing the cross section coefficients calculated above by the cross sectional area of the nanoparticle, the absorption, scattering, and extinction efficiencies (Q_{abs}, Q_{sca}, Q_{ext}) can be found. Figure **1-3** illustrates the dependence of each of these components on the nanoparticle's size. At smaller dimensions (D < 20 nm), the absorption is the greatest contributor to the nanoparticle's overall extinction; however, as size increases, there is an increasingly larger contribution from the scattering coefficient. As the extinction cross section depends on a particle's volume, a larger particle will exhibit increased radiative damping resulting in scattering.[26] Thus, the most efficient conversion of light to heat occurs for particles with a diameter of < 10 nm.[27] However, it is also important to understand how the absorbed light is ultimately converted to heat – that is the photophysics associated with absorption by the SPR.

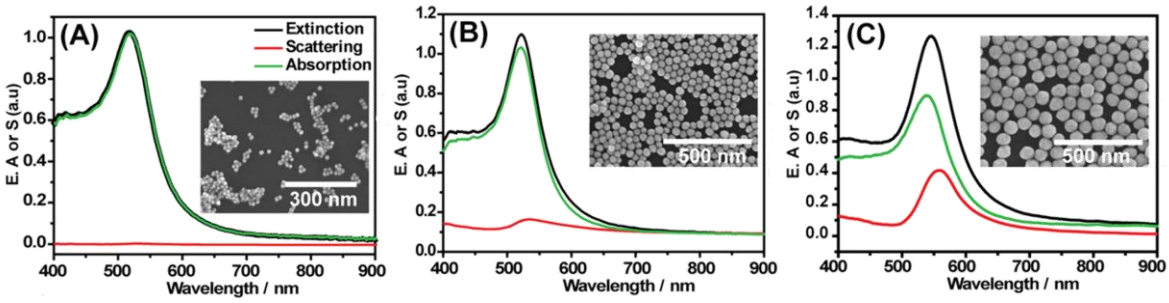

Figure **1-3**: Extracted absorption and scattering spectra for gold nanoparticles of diameters a) 16.5 nm, b) 41 nm, and c) 72 nm.[27]

Photophysics of Light Absorption by Metal Nanoparticles

When the SPR of a nanoparticle is excited, several sequential phenomena take place. The initial response is the creation of a strong electric field from the resonant oscillation of excited free conduction electrons on the particle's surface.[29] This effect is akin to transforming the nanoparticle into a receiver that can be paired with an attached or nearby (< 2 nm away) transmitter molecule.[30] This is, perhaps, the most widely appreciated effect of SPR excitation, as these large fields enhance the interaction of nearby molecules with the incident light via energy transfer from a dipole-dipole interaction.[31] This interaction of the plasmon-induced electric field with nearby molecules has been utilized in a number of applications, including plasmon sensor designs, where the nanoparticles behave as plasmon lasers and the energy transfer is realized as optical gain in emission.[32-34]

Over a period of ~10 fs following excitation, the dipolar oscillation quickly dephases via radiative or non-radiative channels in a manner that depends on the particle size.[23] In particles with a diameter > 10 nm, dephasing of the plasmon can result in radiative decay, emitting a photon that is observed as scattered light. This radiative pathway has been exploited in a number of applications such as surface enhanced Raman as well as optical sensing and bioimaging.[35.36] On the other hand, particles with a diameter < 10 nm primarily dephase via nonradiative decay – a result of inelastic electron-electron scattering.[37] This scattering raises the energy of one of the colliding electrons (and lowers the other), forming an excited-state electron-hole pair. This can occur multiple times, resulting in a large distribution of electron-hole pairs spanning an energy range of several electron volts within a single particle. In a sense, this is the conversion of light energy to electric potential energy. This electric potential energy can provide the driving force for electron transfer to or from the AuNP and has been exploited in splitting water and dissociating H_2.[38-40]

The final photophysical processes that follows excitation of the SPR is the ultimate thermalization of the absorbed energy. The electron potential energy not consumed by electron transfer returns to the equilibrium Fermi-Dirac distribution, dumping the energy of the electrons into the phonons of the metal.[41] Because the excited electrons are produced on a fast timescale (~100 fs) and because the heat capacity of the electrons (C_e) is very small compared to that of the lattice (C_l), the electrons are heated to very high temperatures in a short amount of time, while the lattice remains relatively cool.[41,42] Therefore, in the electron-phonon coupling step, the hot electrons and the phonons are treated as two separate systems whose coupling is described by the two-temperature model (TTM). This model gives the rate of energy exchange between the electrons and phonons in the following coupled equations

$$C_e(T_e)\frac{dT_e}{dt} = -g(T_e - T_l) \tag{1-9}$$

$$C_l\frac{dT_l}{dt} = g(T_e - T_l) \tag{1-10}$$

where T_e and T_l are the electronic and lattice temperatures and g is the electron-phonon coupling constant.[22,40] The electronic heat capacity C_e is assumed to vary linearly with electronic temperature T_e, which means that the timescale of electron-phonon coupling depends on the initial electronic temperature.[43-45] Electron-phonon coupling occurs over ~1 ps ultimately results in an increased temperature for the nanoparticle.

The thermal energy now contained in the lattice of the particle can then diffuse away from the particle raising the local temperature and driving thermally activated transformations. This is the source of the photothermal effect (Scheme **1-1**), which has been used to decompose organic molecules, melt DNA, ablate cancer cells, and is the focus of this dissertation.[46-48] However, to fully understand the ability of the photothermal effect to impart change in the environment, we need to move beyond the generation of this heat to an understanding of the spatial and temporal distribution that results from the diffusion of this heat.

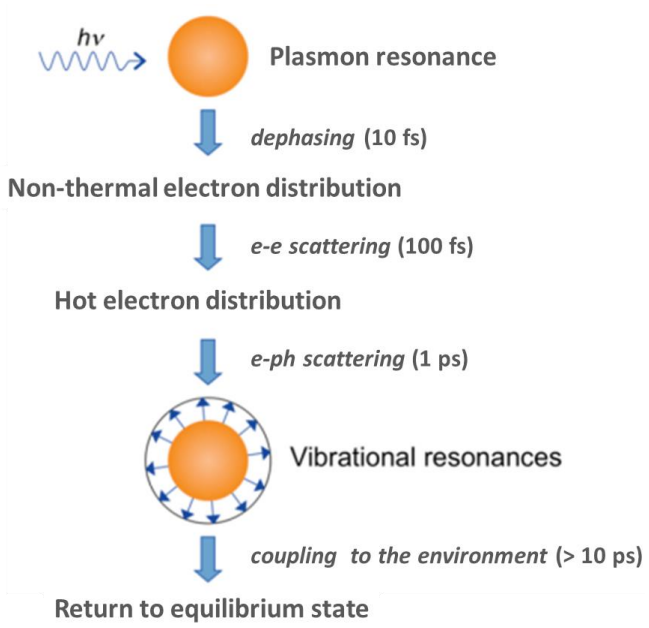

Scheme **1-1**: Sequence of events and approximate timescales following absorption of photons by a metal nanoparticle.[49]

The Photothermal Effect in Time and Space

While the mechanism for generating a photothermal effect in plasmonic nanoparticles is known, in order to establish photothermal heat as a viable alternative heat source, it is important to understand how this heat is transferred to the surroundings and reactive molecules. The following equations govern the temperature of a sphere (nanoparticle) and the heat transfer to its surroundings

$$\frac{\partial T_p}{\partial t} = \frac{\alpha_p}{r}\frac{\partial^2}{\partial r^2}\left[rT_p(r,t)\right] \quad (1\text{-}11)$$

$$\frac{\partial T_s}{\partial t} = \frac{\alpha_s}{r}\frac{\partial^2}{\partial r^2}\left[rT_s(r,t)\right] \quad (1\text{-}12)$$

where the subscript *p* refers to the particle and *s* to the solvent, α is the thermal diffusivity, which is related to the thermal conductivity *k* by $\alpha = k/\rho C_p$, where ρ is the density and C_p is the heat capacity.[49] Using Laplace transform techniques, these equations can be solved together to determine the rate of cooling of the particle.[50-52] Solutions to these heat transfer equations are

more extensively discussed elsewhere, and are illustrated in Figure **1-4** for nanoparticles of different radii.[53]

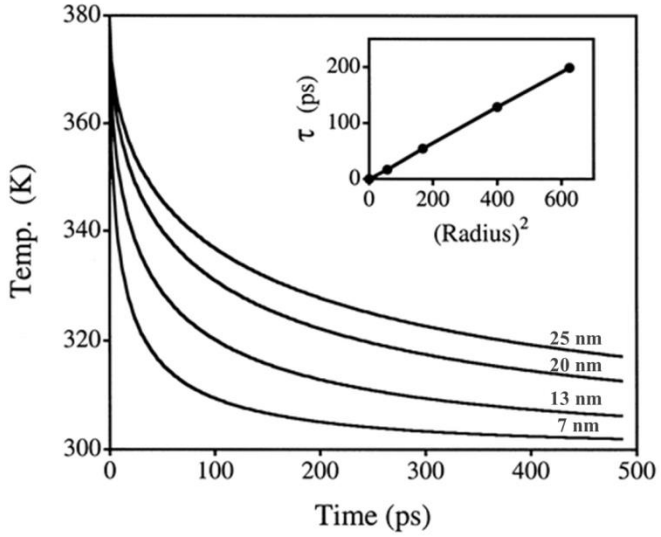

Figure **1-4**: Calculated thermal responses of various sized nanoparticles.[53] From top to bottom, the different traces correspond to particles with radii of 25, 20, 13, and 7 nm. The inset shows the characteristic time constant for energy dissipation (τ) plotted versus the square of the radius.[49]

The thermal response shown in Figure **1-5** can be fit to a stretched exponential function:

$$F(t) = Te^{-(t/\tau)^{\beta}} \qquad (1\text{-}13)$$

where T is the temperature as calculated from the change in sample absorbance, τ is the characteristic time constant energy dissipation, and β is the stretching parameter.[49] The plot in Figure **1-5** shows that $\tau \propto r^2$; thus, heat will dissipate faster in smaller nanoparticles due to their large surface-to-volume ratios. The fast heating and cooling of small nanoparticles translates to greater control over heat delivery, and it also decreases heat accumulation within the nanoparticle, which can result in nanoparticle reshaping or Columbic explosion.[54]

While heat dissipates from the particle at a rate proportional to r^2, the spatial temperature distribution near the particle decays in a manner dependent on the following equation:

$$\Delta T = \frac{q}{kS} \quad (1\text{-}14)$$

where ΔT represents the temperature limits, q is the heat-transfer rate, k is the thermal conductivity, and S is the shape factor, which for a sphere is $4\pi r$.[55] Therefore, the temperature gradient is proportional to $1/r$, where r is the distance from the particle surface. Together, we see that smaller particles result in faster cooling and tighter distributions of temperature near the particles. Thus, the size of nanoparticles is a convenient tool for controlling photothermal impact in time and space.

Controlling Heat Production at the Molecular Level Using Gold Nanoparticles

As seen above, the temporal and spatial evolution of the photothermal effect is dependent upon the size for the nanoparticles. Convenient synthetic methods for AuNPs enable the use of nanoparticles that will provide heat with a precision that approaches the molecular time and length scales. For example, 2 nm particles are very simple to prepare and will exhibit intense temperatures within ~2 nm of their surface, and this heat will dissipate from the particle surface over a period of ~10 ps. Utilizing these nanoparticles to provide high temperatures has many benefits.

Matching the scale of AuNPs to the scale of molecules allows heat to be applied directly to reactive molecules while decreasing the volume of solution heated to that of the immediate nanoparticle surrounding, ensuring more efficient use of heat. This also allows high temperature reactions to be performed under ambient conditions, which is ideal for reactions traditionally carried out in low boiling solvents or on heat sensitive substrates. The disparity in the timescale at which heat is provided compared to the time that is required for the reaction to proceed is also addressed by plasmonic heat. Reactions that were previously heated for hours or even days at a time can instead be heated on timescales that are commiserate with the elementary steps (10^{-15} to

10^{-9} seconds).[56] Considering the timescale of the photophysical event responsible for producing plasmonic heat occurs within ~1 ns (Scheme **1-1**) as well as the rapid rate of cooling (~10 ps) (Figure **1-4**), the photothermal effect dramatically reduces the timescale on which heat is applied as well as opportunities for spurious reactions to occur.

Finally, it is worth commenting on the particular advantages of nanoparticles over other photothermal converters (such as molecules). While it is true that non-emissive dyes are capable of producing a photothermal effect, this effect is limited by the absorptive strength of the dye, the small thermal mass, and the fact that the dyes are only able to absorb 1-2 photons of light at a time. In contrast, nanoparticles possess extinction coefficients three to four times greater than those of strong absorbing organic dyes, making them extremely efficient light absorbers.[12] Small plasmonic particles (< 10 nm) convert nearly all of this absorbed light into heat, have a large thermal mass, can absorb multiple photons at a time, and are capable of reaching temperatures in excess of 1000 K.[57] While such extreme temperatures are not necessary for most reactions, and are in fact deleterious to most, the highly localized and transient nature of plasmonic heat (< 20 nm) may avoid undesired reactions and allow access to temperatures previously forbidden in various solutions and substrates. These high temperatures, coupled with matching of the size and timescale of the heat source to that of the reactive molecules, transform heat into a spatially and temporally precise, on-demand synthetic tool. Thus, the potential for plasmonic heat to provide well-controlled and effective heat is great, but further understanding of how to apply it to a large range of reactions is required. That is the objective of this dissertation.

Dissertation Overview

The work in this dissertation contributes to a better understanding the ability of nanoparticles to impart heat to a molecular system with the ultimate goal of transforming plasmonic heat into a controlled synthetic tool. We are interested in exploring the extent of

control we can exercise over plasmonic heat so that we may establish plasmonic heat as a means promote to a variety of reaction types at various temperatures. To achieve this goal, we have investigated both solution and solid state reactions, and both making and breaking chemical bonds.

In Chapter **2**, I will discuss the decision to work with 2 nm gold nanoparticles under pulsed irradiation, and examine their ability to thermally decompose a solid polymer into its volatile products. The kinetics of this reaction will be utilized to propose temperatures occurring at the nanoparticle surface, and compare these values to theoretically determined temperatures. With a better understanding of the temperatures achieved in a solid medium, I will then illustrate ability of plasmonic heat to constructively promote chemical reactions. In Chapter **3**, the rate of formation of a polyurethane generated via plasmonic heating will be compared to the rate of formation with a common catalyst, as well as their ability to form bonds synergistically. Chapter **4** will discuss gold nanoparticles as photothermal agents as well as examine other nanoparticle materials. The final chapter of this dissertation summarizes the conclusions from each project, and discusses future that will serve to demonstrate our ability to provide plasmonic heat to a wide range of chemical reactions. In its entirety, this dissertation will provide the scientific community with insight into a novel synthetic tool equal in effectiveness and superior in control to current synthetic heating methods.

References

1. Yang, H.; Malik, R.; Narasimha, S. & Li, Y. Dual Stress Liner for High Performance Sub-45nm Gate Length SOI CMOS manufacturing. *Electron Devices Meeting, IEDM Technical Digest, IEEE International*, 1075-1077 (2004).
2. Betancourt, T. & Brannon-Peppas, L. Micro-and Nanofabrication Methods in Nanotechnological Medical and Pharmaceutical Devices. *Int. J. Nanomed.*, **4**, 483-495 (2006).
3. Pennisi, E. The CRISPR Craze. *Science*, **341** 833-836 (2013).
4. Botte, G. G. Electrolytic cells and methods for the production of ammonia and hydrogen. U.S. Patent US20090095636 A1, April 16, 2009.
5. Del Bianco, A.; Panariti, N.; Anelli, M.; Beltrame, P.L. & Carniti, P. Thermal cracking of petroleum residues. *Fuel*, **72**, January 1993, 75–80 (1993).
6. Bakhtiari, A.; Hsiao, D.; Jin, G.; Gates, B. & Branda, N. An Efficient Method Based on the Photothermal Effect for the Release of Molecules from Metal Nanoparticle Surfaces. *Angew. Chem. Int. Edit.* **48**, 4166-4169 (2009).
7. Gheneim, R.; Perez-Berumen, C. & Gandini, A. Diels-Alder reactions with novel polymeric dienes and dienophiles: Synthesis of reversibly cross-linked elastomers. *Macromolecules* **35**, 7246–7253 (2002).
8. Chen, X.; Wudl, F.; Mal, A. K.; Shen, H. & Nutt, S. R. New thermally remendable highly cross-linked polymeric materials. *Macromolecules* **36**, 1802–1807 (2003).
9. Engel, T. & Kickelbick, G. Thermoreversible Reactions on Inorganic Nanoparticle Surfaces: Diels–Alder Reactions on Sterically Crowded Surfaces. *Chem. Mater.* **25**, 149-157 (2012).
10. Osborn, J.A. & Schrock, R.R. Coordinatively unsaturated cationic complexes of rhodium(I), iridium(I), palladium(II), and platinum(II). Generation, synthetic utility, and some catalytic studies. *J. Am. Chem. Soc.*, **93**, 3089–3091 (1971).
11. Kappe, C. Controlled microwave heating in modern organic synthesis. *Angew. Chem. Int. Ed.* **43**, 6250-6284 (2004).
12. Link, S. & El-Sayed, M. A. Shape and Size Dependence of Radiative , Non-Radiative and Photothermal Properties of Gold Nanocrystals. *Int. Rev. Phys. Chem.* **19**, 409-453 (2000).
13. Gavrilenko, V.I. *Optics of Nanomaterials* (Pan Stanford Publishing, Singapore, 2011).
14. Linic, S., Christopher, P. & Ingram, D. B. Plasmonic-metal nanostructures for efficient conversion of solar to chemical energy. *Nat. Mater.* **10**, 911-921 (2011).
15. Esteban, R.; Borisov, A. G.; Nordlander, P. & Aizpurua, J. Bridging quantum and classical plasmonics with a quantum-corrected model. *Nat.Commun.* **3**, 825-8 (2012).
16. Savage, K. J.; Hawkeye, M. M.; Esteban, R.; Borisov, A. G.;Aizpurua, J. & Baumberg, J. J. Revealing the quantum regime in tunnelling plasmonics. *Nature* **491**, 574−577 (2012).
17. Kerker, M. The optics of colloidal silver: something old and something new *J. Colloid Interface Sci.* **105**, 297-314 (1985).
18. Link, S. & El-Sayed, M. A. Spectral Properties and Relaxation Dynamics of Surface Plasmon Electronic Oscillations in Gold and Silver Nanodots and Nanorods. *J. Phys. Chem. B* **103**, 1-17 (1999).
19. Williams, M. A. & Daviter, T. *Protein-Ligand Interactions Methods and Applications 2nd Ed.* (Humana Press, New York, 2013).
20. Campbell, C. & Kim, G. SPR microscopy and its applications to high-throughput analyses of biomolecular binding events and their kinetics. *Biomaterials* **28**, 2380-2392 (2007).

21. Mie, G. Contributions to the Optics of Turbid Media, Particularly of Colloidal Metal Solutions. *Ann. Phys.* **25**, 377-445 (1908).
22. Link, S. & El-Sayed, M. A. Size and Temperature Dependence of the Plasmon Absorption of Colloidal Gold Nanoparticles. *J. Phys. Chem. B* **103**, 4212-4217 (1999).
23. Hartland, G. V. Optical studies of dynamics in noble metal nanostructures. *Chem. Rev.* **111**, 3858-3887 (2011).
24. Bartschat, K. *Computational Atomic Physics: Electron and Positron Collisions with Atoms and Ions* (Springer, New York City, 1996).
25. Kreibig, U. & Vollmer, M. *Optical Properties of Metal Clusters* (Springer-Verlag, Berlin, 1995).
26. Grigorchuk, N. Radiative damping of surface plasmon resonance in spheroidal metallic nanoparticle embedded in a dielectric medium. *J. Opt. Soc. Am. B* **29**, 3404-3411 (2012).
27. Liu, B.; Lin, K.; Hu, S.; Wang, X.; Lei, Z.; Lin, H. and Ren, B. Extraction of Absorption and Scattering Contribution of Metallic Nanoparticles Toward Rational Synthesis and Application. *Anal. Chem.* **87**, 1058-1065 (2015).
28. Jain, P. K.; Lee, K. S.; El-Sayed, I. H. & El-Sayed, M. A. Calculated absorption and scattering properties of gold nanoparticles of different size, shape, and composition: applications in biological imaging and biomedicine. *J. Phys. Chem. B* **110**, 7238-7248 (2006).
29. Moores, A. & Goettmann, F. The plasmon band in noble metal nanoparticles: an introduction to theory and applications. *New J. Chem.* **30**, 1121–1132 (2006).
30. Pacioni, N. L.; González-Béjar, M.; Alarcón, E.; McGilvray, K. L. & Scaiano, J. C. Surface Plasmons Control the Dynamics of Excited Triplet States in the Presence of Gold Nanoparticles. *J. Am. Chem. Soc.* **132**, 6298-6299 (2010).
31. Scaiano, J. C. & Stamplecoskie, K. Can Surface Plasmon Fields Provide a New Way to Photosensitize Organic Photoreactions? From Designer Nanoparticles to Custom Applications. *J. Phys. Chem. Lett.* **4**, 1177-1187 (2013).
32. Berini, P. & DeLeon, I. Surface Plasmon–Polariton Amplifiers and Lasers *Nat. Photonics* **6**, 16– 24 (2012).
33. Seidel, J.; Grafström, S. & Eng, L. Stimulated Emission of Surface Plasmons at the Interface between a Silver Film and an Optically Pumped Dye Solution *Phys. Rev. Lett.* **94**, 177401 (2005).
34. Noginov, M. A.; Zhu, G.; Belgrave, A. M.; Bakker, R.; Shalaev, V. M.; Narimanov, E. E.; Stout, S.; Herz, E.; Suteewong, T.& Wiesner, U. Demonstration of a Spaser-Based Nanolaser *Nature* **460**, 1110– 1112 (2009).
35. Novo, C.; Funston, A. M. & Mulvaney, P. Direct observation of chemical reactions on single gold nanocrystals using surface plasmon spectroscopy. *Nat. Nanotechnol*. **3**, 598–602 (2008).
36. Sokolov, K.; Follen, M.; Aaron, J.; Pavlova, I.; Malpica, A.; Lotan, R. & Richards-Kortum, R. Real-time vital optical imaging of precancer using anti-epidermal growth factor receptor antibodies conjugated to gold nanoparticles. *Cancer Res*. **63**, 1999– 2004 (2003).
37. Klar, T.; Perner, M.; Grosse, S.; von Plessen, G.; Spirkl, W. & Feldmann, J. Surface-plasmon resonances in single metallic nanoparticles. *Phys. Rev. Lett.* **80**,4249–4252 (1998).
38. Mukherjee, S. et al. Hot Electrons Do the Impossible: Plasmon-Induced Dissociation of H_2 on Au. *Nano Lett.* **13**, 240-247 (2013).
39. Thomann, I.; Pinaud, B. A.; Chen, Z.; Clemens, B. M.; Jaramillo, T. F. & Brongersma, M. L. Plasmon Enhanced Solar-to-Fuel Energy Conversion. *Nano Lett.* **11**, 3440– 3446 (2011).

40. Chen, H. M.; Chen, C. K.; Chen, C.-J.; Cheng, L.-C.; Wu, P. C.; Cheng, B. H.; Ho, Y. Z.; Tseng, M. L.; Hsu, Y.-Y.; Chan, T.-S.; Lee, J.-F.; Liu, R.-S. & Tsai, D. P. Plasmon Inducing Effects for Enhanced Photoelectrochemical Water Splitting: X-ray Absorption Approach to Electronic Structures. *ACS Nano* **6**, 7362– 7372 (2012).
41. Qiu, T. Q. & Tien, C. L. Short-pulse laser heating on metals. *International Journal of Heat Mass Transfer* **35**, 719-726 (1992).
42. Anisimov, L.; Kapeliovich, B. L. & Perelman, T. L., Electron emission from metal surfaces exposed to ultrashort laser pulses. *Soviet Phys. JETP* **39**, 375-377 (1974).
43. Hodak, J. H.; Henglein, A. & Hartland, G. V. Photophysics of Nanometer Sized Metal Particles: Electron−Phonon Coupling and Coherent Excitation of Breathing Vibrational Modes *J. Phys. Chem. B* **104**, 9954-9965 (2000).
44. Hodak, J. H.; Martini, I. & Hartland, G. V. Ultrafast study of electron–phonon coupling in colloidal gold particles. *Chem. Phys. Lett.* **284**, 135-141 (1998).
45. Hodak, J. H.; Henglein, A. & Hartland, G. V. Electron-phonon coupling dynamics in very small (between 2 and 8 nm diameter) Au nanoparticles. *J. Chem. Phys*. **112**, 5942-5947 (2000).
46. Fasciani, C., Alejo, C. J., Grenier, M., Netto-Ferreira, J. C. & Scaiano, J. C. High-temperature organic reactions at room temperature using plasmon excitation: decomposition of dicumyl peroxide. *Org. Lett.* **13**, 204-207 (2011).
47. Huschka, R.; Zuloaga, J.; Knight, M. W.; Brown, L. V.; Nordlander, P. & Halas, N. J. Light-Induced Release of DNA from Gold Nanoparticles: Nanoshells and Nanorods *J. Am. Chem. Soc.* **133**,12247– 12255 (2011).
48. Dreaden, E. C., Mackey, M. A., Huang, X., Bin Kang & El-Sayed, M. A. Beating cancer in multiple ways using nanogold. *Chem. Soc. Rev.* **40**, 3391-3404 (2011).
49. Hu, M. & Hartland, G. V. Heat Dissipation for Au Particles in Aqueous Solution : Relaxation Time versus Size. *J. Phys. Chem. B* **106**, 7029-7033 (2002).
50. Plech, A.; Kotaidis, V.; Gresillon, S.; Dahmen, C. & von Plessen, G. Laser-induced heating and melting of gold nanoparticles studied by time-resolved x-ray scattering *Phys. Rev. B* **70**, 195423 (2004)
51. Perrin, B. Investigation of Short-Time Heat Transfer Effects by an Optical Pump–Probe Method. *Top. Appl. Phys.* **107**, 333-359 (2007).
52. Juve, V.; Scardamaglia, M.; Maioli, P.; Crut, A.; Merabia, S.; Joly, L.; Del Fatti, N. & Vallee, F. Cooling dynamics and thermal interface resistance of glass-embedded metal nanoparticles. *Phys. Rev. B* **80**, 195406 (2009)
53. Cooper, F. Heat Transfer from a Sphere to an Infinite Medium . *Int. J. Heat Mass Transfer* **00**, 991-993 (1977)
54. Werner, D.; Hashimoto, S. &Uwada, T. Remarkable photothermal effect of interband excitation on nanosecond laser-induced reshaping and size reduction of pseudospherical gold nanoparticles in aqueous solution. *Langmuir* **26**, 9956-9963 (2010).
55. Holman, J. P. *Heat Transfer 8th Ed.* (McGraw-Hill, New York, 1997).
56. Turro, N. J.; Ramamurthy, V. & Scaiano, J.C. *Principles of Molecular Photochemistry* (University Science Books, Sausalito, 2009).
57. Nedyalkov, N. N., Imamova. S.E., Atanasova, P.A., Toshkova, R.A., Gardeva, E.G., Yossifova, L.S., Alexandrov, M.T., Obara, M.. Interaction of gold nanoparticles with nanosecond laser pulses: Nanoparticle heating. *Appl. Surf. Sci.* **257**, 5456-5459 (2011).

Chapter 2

Using Reaction Kinetics to Determine Photothermal Temperatures

Introduction

To increase the effectiveness and efficiency of heat as a synthetic tool, we must increase our control over its placement, timing, and quantity. As mentioned in Chapter **1**, conventional heating methods possess these qualities only in a very limited sense. Heat is applied to the desired reaction, but it is also supplied to the environment and other non-reactive thermal absorbers, and once the appropriate reaction temperature is reached, this temperature must be maintained for minutes, hours, or even days. By providing heat on the molecular level at timescales matching that of elementary steps of reaction (i.e. bond breaking and bond formation), we can increase spatial and temporal control over heating.

Over the last decade, the photothermal effect has received increasing interest for its ability to provide heat. Nanoparticles can quickly and efficiently convert light into intense heat, reaching up to several thousands of degrees.[1] Due to the mismatch between rates of vapor nucleation and thermal diffusion, these temperatures exist within the solvent, allowing even solution phase reactions to be run at these high temperatures. In addition, the heat produced then decays over several nanometers of distance from the particle surface, allowing for high temperature reactions to proceed near the particle while the bulk experiences only mild temperature increases. Plasmonic heat has been utilized in solution-based systems such as drug delivery, cancer therapy, and high temperature organic reactions[2,3] However, these applications have demonstrated limited characterization of the timing and placement of heat. To understand the control we have over the heat generated, we can follow the kinetics of a photothermally driven reaction and then use these kinetics to define the temperatures produced by plasmonic

nanoparticles. Using this approach we can begin to understand and tailor the properties that influence heat production.

While many of the prior studies involving plasmonic heating investigated applications in solution, plasmonic heat also promises advantages for solid state transformations.[2,3] Many bulk properties (magnetism, conductivity, etc.) are temperature dependent, and the ability to drive chemical reactions with large activation barriers while maintaining a low bulk temperature (and therefore preserving desired bulk properties) is attractive. The advantages of plasmonic heating for effecting solid-state transitions have not gone unnoticed.[4-11] Recent demonstrations of modifications to surfaces have established plasmonic heating as a viable and efficient means for promoting solid state change on the nanoscale. For instance, Alessandri and co-workers exploited plasmonic heat to "write" with a laser by ablating a polymeric surface coated in gold nanoparticles.[6] Imparting physical changes to a surface has also been utilized in high-speed memory storage devices and selective defect healing, and has the advantage of facile characterization techniques such as differential scanning calorimetry and differential thermal analysis.[4,11] Though these reports demonstrate the ability of plasmonic heat to drive physical changes, they provide limited insight into the reaction kinetics and reaction mechanisms, both of which are important for determining temperatures obtained by excited nanoparticles as well as any advantage plasmonic heating may impart. In order to determine these, it becomes important to collect and characterize reaction products so that a known reaction pathway can be inferred. By following the kinetics of the thermal decomposition of a polymer, the reaction's rate, efficiency, and temperatures achieved via the photothermal effect can be elucidated.

Choosing a Model System for Bond Cleavage

In order to study kinetics of photothermally driven reactions, we employed solid films of polypropylene carbonate (PPC) containing heptane thiol-protected gold nanoparticles (average

diameter ~ 2 nm). The decision to work with PPC stems from both its wide spread application in a variety of materials as well as its chemical behavior. PPC is a robust and versatile polymer, commonly employed to increase the toughness in some epoxy resins, as well as in packaging, medical materials, and laboratory equipment.[12] However, the low cost of PPC means that many of these materials are often considered disposable, and are thrown away at the end of their short lifespan. While the product may have a short lifespan, the polymer does not, and it can take years for the material to fully decompose. Though recycling of PPC is available, it requires a costly melting process at high temperatures (> 240°C).[13] Despite the desire to decrease the volume of materials in landfills, the melting process employed in recycling is both financially and energetically costly. If efficiency is increased, then consumers are more likely to recycle. Thus, recycling efforts stand to benefit from improved heating methods, such as plasmonic heating.

PPC also has many chemical properties that make this system well suited for following the impact of photothermal heating. First, the bulk thermal decomposition is clean, so that we can expect a clean photothermal reaction. The clean reaction also means that the thermodynamic and kinetic parameters for the thermal decomposition of PPC have been determined. The thermal decomposition of PPC exhibits two high barrier decomposition mechanisms: chain unzipping (124 kJ/mol) and chain scission (185 kJ/mol) (Scheme **2-1**).[14,15] The high barriers for these transformations mean that the rate and room temperature is negligible, and that we can ascribe any decomposition of PPC to photothermal heating. For these two reactions, chain unzipping predominantly generates propylene carbonate (PC) monomer, which has significant volatility. Chain scission functions to cleave the backbone of the polymer, forming two shorter oligomers, which may then undergo further chain scission or unzipping. In either case, we expect a clean thermal reaction that produces a final product of volatile monomers. The production of a volatile monomer provides a simple means by which to follow the course of reaction: we can associate mass loss of the film with thermal decomposition. Additionally, the first order nature of both of

these mechanisms simplifies the kinetic analysis and temperature calculations. Finally, PPC is colorless, so it has negligible intrinsic photothermal behavior.

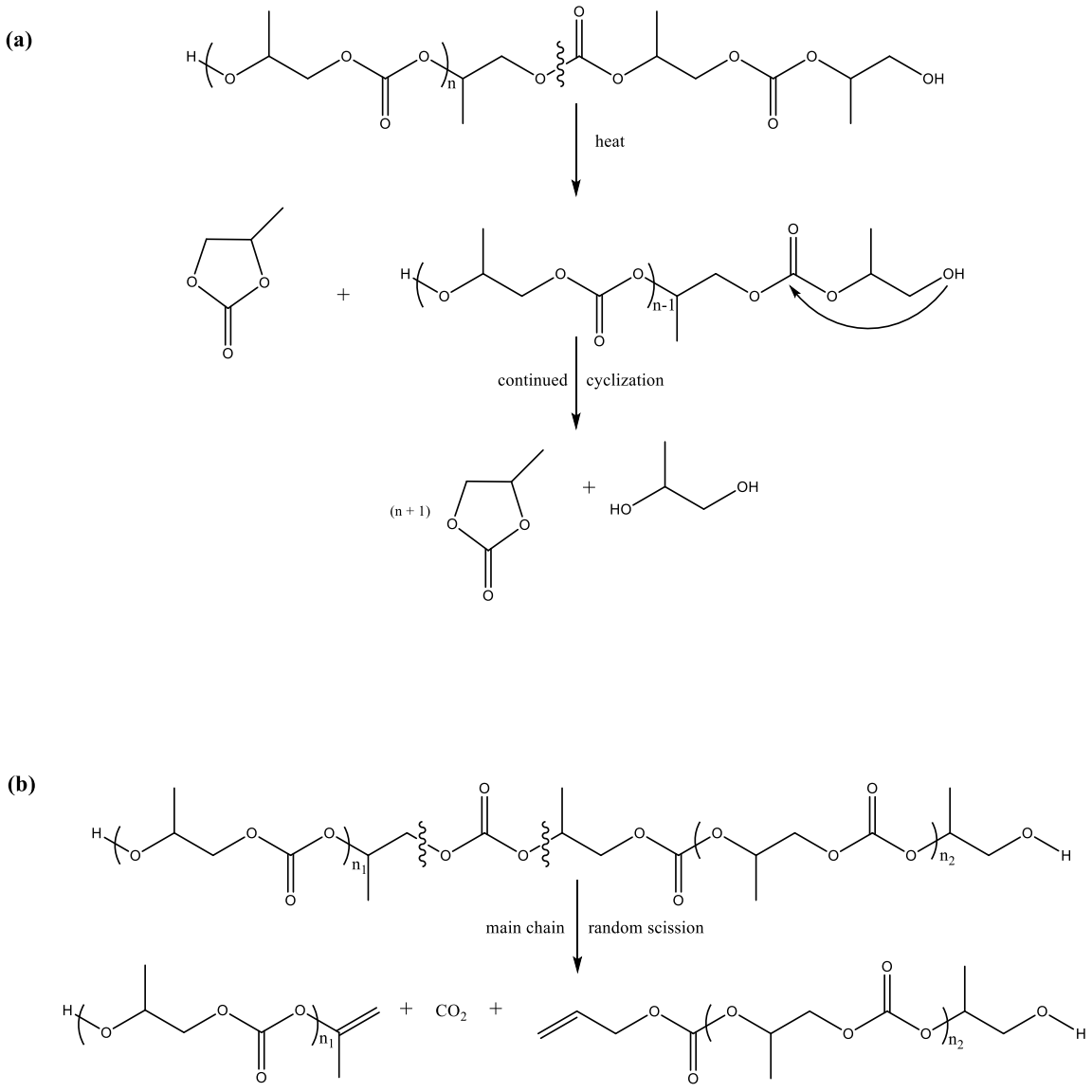

Scheme **2-1**. The thermal decomposition of PPC occurs via (a) chain unzipping at 220°C (E_a=124 kJ/mol) and (b) random chain scission at 247°C (E_a=185 kJ/mol).[14,15]

Choosing a Photothermal Agent

With a reactant chosen, we next needed to select the photothermal agent. For this work, we chose 2 nm gold nanoparticles (AuNPs) as our plasmonic heat source. The decision to work with small nanoparticles is two-fold: their high absorption cross section and rapid heat dissipation. AuNPs with dimensions < 20 nm exhibit an extinction that is dominated by absorption, which is essential to eliciting a photothermal response.[16] By decreasing the amount of light scattered, we can ensure that a majority of light interacting with the particles has the potential for conversion to heat. While it is important for this work that the photothermal effect dominate the optical response of the nanoparticle, eliciting the greatest quantity of heat is not of equal importance. AuNPs on the scale of D = 40 nm have a very large Q_{abs} (Figure **1-2**); however, because heat dissipation is proportional to surface area-to-volume ratio, larger particles will also take significantly longer to transfer their heat to the surroundings (Figure **1-1**).[17] In 2 nm AuNPs, nearly 50% of the gold atoms compose the nanoparticle surface, resulting in rapid heat dissipation (~1 ps).[18,19] Rapid heat dissipation is desirable for the ability to quickly provide heat to the desired reactive molecules while also minimizing any thermal fragmentation or reshaping of the AuNPs that could occur from retention of heat on a longer timescale. It is important to prevent any change in size or shape to the AuNPs so that the SPR, which is sensitive to these properties, remains unchanged; thereby maintaining control over optical absorption by the AuNPs. Furthermore, the small size of the nanoparticle and localized nature of plasmonic heat intrinsically make spatial control highly precise; the rapid rate of heating and cooling means that the nanoparticle generates heat only under periods of irradiation, creating on-demand heat controlled by the light source with picosecond precision. Therefore, in order to maximize absorption while also maximizing heat dissipation to the surroundings, 2 nm AuNPs were chosen.

The surface of nanoparticles is often passivated by a ligand, and this ligand can serve several purposes. Most importantly, surface ligands stabilize nanoparticles, and this can be done

by creating an electrostatic double layer or through steric stabilization.[20] These ligands can help to control the particle's size, inhibit agglomeration and precipitation, and prevent oxidation of the metal.[21] Ligands can also be used to change the solubility, introduce new functionalities, and alter the electronic properties of the particle. For AuNPs, the Au-S bond is the most common motif for attaching ligands to the surface. In this work, we protected our AuNPs with heptane thiol chains. These chains provide sufficient stability to prevent particle aggregation as well as the necessary solubility for incorporation into PPC films.

Characterizing the Product

The samples themselves were formed by dissolving both PPC and AuNPs in CH_2Cl_2. These solutions were drop cast onto pre-weighed glass slides and allowed to dry for 24 hours. The slides were reweighed, exposed to 7,000 pulses (~8 ns pulse width) of 532 nm light from a frequency-doubled Nd:YAG laser and then weighed again. Full experimental and synthetic details, as well as discussions of the optical properties of these films can be found in the Appendix. Exposure to the laser resulted in a loss of material and a change in the color of the film (Figure **2-1a**). We attribute the loss in mass to depolymerization of PPC generating a volatile monomer that is then evaporated. As noted above, the final product of decomposition is the PPC monomer.

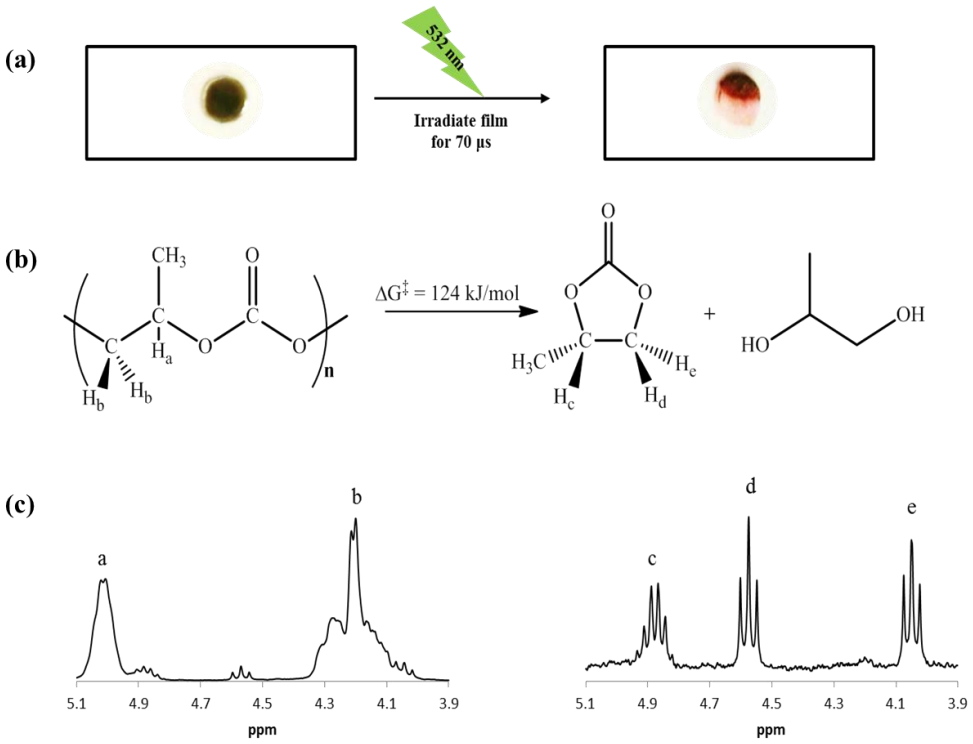

Figure **2-1**. (a) The course of a general experiment. (b) Chemical equation for the depolymerization of polypropylene carbonate (PPC) by chain unzipping. (c) 1H NMR of the polymer blend before (left) and after (right) irradiation.[22]

The proposed analysis rests upon the assumption that we are driving the chemical transformation from polymer to monomer during laser excitation, and the validity of this assumption was confirmed by exposing a film with a nanoparticle concentration [*np*] of 9.9 x 10^{-3} (mass fraction) in a sealed vial to laser irradiation. In addition to an evident mass loss of the solid, a clear liquid and gas were produced within the vial. The contents of the vial were then extracted with deuterated chloroform. Subsequent analysis using ^{1}H NMR indicated that the resulting liquid and gas were predominantly monomer. Figure **2-1c** shows a comparison of the ^{1}H NMR spectra of the polymer/nanoparticle films before and after irradiation. The spectrum of the as-prepared polymer and nanoparticle mixture before irradiation (Fig **2-1c** left) contains prominent methylene peaks at 4.20 and 4.99 ppm that are attributed to protons characteristic of the polymer In contrast, after irradiation (Fig **2-1c** right) these peaks disappear and a quartet at

4.85 and triplets at 4.58 and 4.02 ppm belonging to the monomer become distinct. These results are consistent with the degradation of the polymer to the monomer. The fact that the only chemicals we detected were the polymer and monomer indicates a clean chemical degradation and we feel confident in ascribing the mass losses in the polymer film to the generation and subsequent evaporation of monomer. In addition, this constituted the first demonstration of a solid-state chemical transformation, driven by plasmonic heating, in which both the reactants and products are known, setting the stage for kinetic analyses of the transformation.

Confirming the Photothermal Effect of Gold Nanoparticles

Before the kinetic analysis, it is first necessary to confirm that the photothermal effect of the nanoparticles is responsible for the degradation of the film. To this end, we performed an intensity study (Figure **2-2**), in which the energy of the laser was varied from 20 mJ to 200 mJ. For our laser, this corresponds to an incident intensity from 5 MW/cm^2 to 50 MW/cm^2. We found that the % decomposition of polymer varied roughly linearly with the intensity of the laser pulse, which is expected at the extreme temperatures obtained by the particles (*vide infra*).

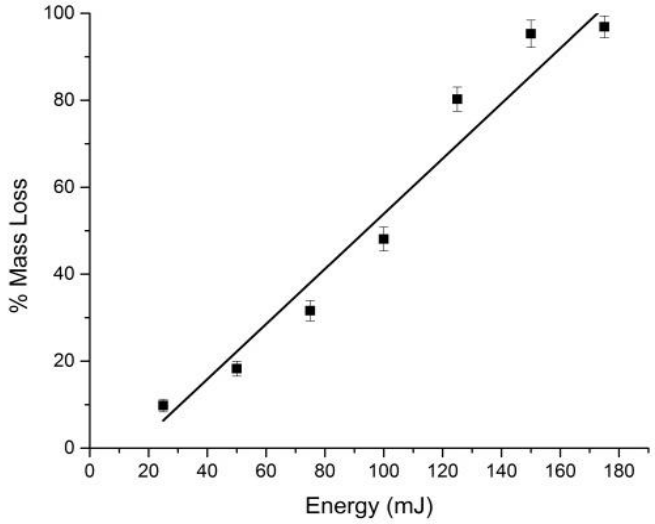

Figure **2-2**. Change in mass loss (% decomposition) as a function of incident laser energy (intensity). Also shown is a linear regression fit to this data.[22]

Further evidence for the nanoparticles being the source of heat driving the decomposition of the polymer is found in Figure **2-3**. This plot reports the results of a study into the dependence of the % PPC degradation upon the [*np*]. For this study, the [*np*] was determined by mass fraction of the film. In the absence of gold nanoparticles, the mass loss of the film was small (3.42%), but non-zero. Of note, in Figure **2-3**, is that the percent completion of the decomposition does not monotonically increase with [*np*]. Instead, we observed a levelling off of the efficiency of driving the thermal decomposition of PPC at higher [*np*]. This behavior can be explained by considering that the heat needed to drive the thermal decomposition of the film is directly related to the energy of light absorbed. The energy of light absorbed is the product of the intensity of light, the volume illuminated by the light, and the concentration of light absorbers ([*np*]). We must also consider that the beam of light is attenuated by the sample. Thus, for a cylindrical beam of light (radius, *r*) passing through a sample of thickness, *l*, the total energy absorbed is given by:

$$\int_0^l I_0 10^{-\varepsilon[np]l}(\pi r^2 l)[np]dl \qquad (2\text{-}1)$$

where ε is the extinction coefficient associated with the nanoparticles and I_0 is the intensity of the light at the surface of the sample. Due to the inherent heterogeneity of nanoparticles, we made no attempt to determine ε in terms of molarity. However, we do calculate ε, in terms of mass fraction, to be 0.641 mg_{film} mg_{np}^{-1} μm^{-1} at 532 nm (see Appendix). Integration of Equation **2-1** yields the energy absorbed (related to the temperature produced) in relation to [*np*], which was used to produce the fitted curve in Figure **2-3**. The values from Figure **2-3** are shown in Table **2-1.**

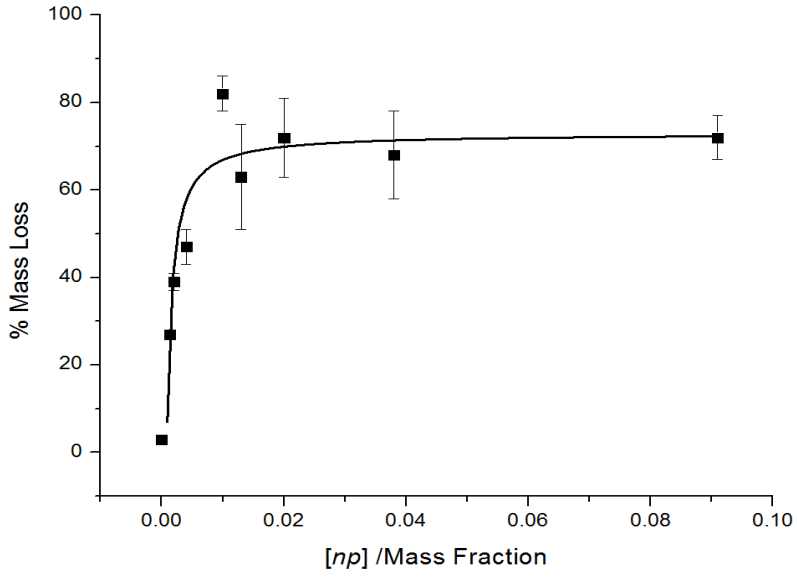

Figure **2-3**. Change in the % mass loss versus mass fraction (concentration) of gold nanoparticles. Equation 1 is fit to this data (black curve).[22]

Table **2-1**. Concentrations of AuNPs in films (given as mass fraction) and the observed % completion of the PPC film upon exposure to our laser. Also given are the standard deviations in these measurements.

AuNP Mass Ratio	***% Decomposition***
9.1×10^{-2}	72 ± 5
3.8×10^{-2}	68 ± 10
2.0×10^{-2}	72 ± 9
1.3×10^{-2}	63 ± 12
9.9×10^{-3}	82 ± 4
4.0×10^{-3}	47 ± 4
2.0×10^{-3}	39 ± 2
1.3×10^{-3}	27 ± 1
0.0	3 ± 1

The behavior of this curve can be explained by a simple physical picture. At low [*np*] the optical density of the film is small enough that the entire thickness of the film experiences significant fluence of photons. In this non-light-limited regime, increasing [*np*] merely increases the number of hot spots – resulting in a linear dependence of percent completion upon [*np*]. However, at high [*np*], the optical density will be large enough that the front portion of the film functions to shield the back portion of the film. In this light-limited regime, the reaction *volume* (the portion of the film exposed to significant fluence of photons) decreases as $[np]^{-1}$, while the sources of heat *within* the shrinking illuminated volume continue to increase linearly with [*np*]. Therefore, these two effects cancel out to give an absorbed energy that is independent of [*np*]. This behavior follows Beer's Law, where increasing concentration corresponds to increased absorption. In our work, increased light absorption corresponds to increased heat production.

Determining Photothermal Temperatures

The demonstration that it is the optical absorption of the AuNPs that provides the driving force for reactions also opens the door for calculation of the kinetics of the reaction. Because we know the mechanisms for decomposition and can characterize the identity and quantity of monomer produced, we can use the Arrhenius equation to estimate the temperatures experienced by irradiated films. For this analysis, we consider the film with a [*np*] of 9.9 x 10^{-3}, though the same approach is valid for all samples. For 2 nm particles, decay of the elevated temperature, post-excitation of the SPR, is extremely rapid.[17, 23] Thus, we assume that elevated temperatures only exist for the duration of the laser pulse (8 ns). Given that the films were exposed to 7,000 pulses, this means that the total reaction time was ≤ 56 μs. We can proceed with calculations based on the first-order kinetics of this reaction. The sample we are considering experienced a 82% completion indicating the passage of 2.4 half-lives – or an observed half-life of 23 μs.

This observed average half-life can be turned into an estimation of the "average" temperature, through use of the Arrhenius equation:

$$k_d = Aexp^{\left(-\frac{\Delta G^{\ddagger}}{RT}\right)} \qquad (2\text{-}2)$$

where k_d is the observed rate of decomposition, $\Delta G^{\ddagger}$ is the activation barrier to decomposition, R is the ideal gas constant, and T is the temperature of the system. We know, from above, the observed rate (taken from the observed half-life), as well as the activation barrier. As the reaction is unimolecular (Figure **2-1a**), we arrive at the conclusion that the pre-exponential factor (A) is controlled by the frequency of the bond that is broken (C-O) in the polymer. For this, we use a typical frequency of this bond (2.4 x 10^{12} s^{-1}). This choice has been experimentally validated.[14] Using this information, we solve for an "average" temperature in the film of *at least* 800 K. This is the temperature that the entire film would be required to reach, assuming a single uniform temperature.

Given the localized nature of the heat produced, and the fact that these films are cool to the touch after irradiation, it seems unlikely that this uniform temperature is actually obtained throughout the film. Rather, this estimate represents a minimum temperature that the system must obtain. In reality, molecules near the surface of the nanoparticles will experience much higher temperatures (and faster decay rates) than those far away from the nanoparticles. An estimate of the peak temperature at the nanoparticle surface may be calculated assuming that all the energy absorbed by the nanoparticle (E_{abs}) is converted to heat, which is responsible for increases in the nanoparticle temperature. The energy absorbed by the nanoparticle is well-described by Mie theory:[24]

$$E_{abs} = \sigma_{abs} \int_0^{pw} I(t)dt \qquad (2\text{-}3)$$

In this equation, σ_{abs} is the absorption coefficient (discussed in Chapter **1**), I is the intensity of the light source, and pw is the pulse width of the laser. This equation predicts that 20.9 x 10^{-17} J is absorbed by our 2 nm particles. Given that 9.77 x 10^{-17} J is required to vaporize a 2 nm gold particle, (initially at room temperature),[‡] this analysis predicts a final temperature above gold's boiling point (3154 K).

It is doubtful that this localized temperature is actually reached either, as dissipation of heat also occurs during the laser pulse.[25, 17] Instead, it seems likely that the actual temperature lies between the two extremes calculated using Equations **2-2** and **2-3**. Nevertheless both of these limiting cases predict extreme temperatures as would be required to drive the degradation of PPC to a significant extent in such a short period of time.

The fact that we are able to drive the reaction to such a significant extent raises another issue: the density of gold is roughly 16 times greater than PPC, and even in the most concentrated film (1:10), the gold will occupy little more than 0.06% of the film's volume. However, despite their small volume and the highly localized nature of plasmonic heat, we observe more than 70% mass loss in these films. This suggests that the polymer must migrate to the nanoparticle (or *vice*

versa) between or during pulses. Either of the temperatures calculated so far are well above the glass transition temperature of PPC,[15] and so is not unexpected, but it is impressive to see that such a small mass fraction can exert such large changes to the film.

The Photothermal Effect of an Organic Dye

Finally, we address the efficiency of nanoparticles for driving chemical reactions by comparing the effectiveness of driving thermal reactions using nanoparticles versus dyes with low quantum yields for luminescence. Such dyes are also quite efficient at converting light to heat and (due to the very small heat capacity of single molecules) are capable of reaching extreme temperatures post-excitation. However, the small heat capacity of these dyes means that they are cannot absorb as much energy as AuNPs, and consequently their thermal effects on the surroundings will also be less than AuNPs. As a result, dyes will effect less degradation on PPC films.

To test this hypothesis, we employed Sudan IV, a well-known dye with an absorption maximum at 520 nm and a quantum yield for luminescence much less than 0.01 (see Appendix). Thus, this dye also efficiently absorbs 532 nm light and converts it to heat. Despite the efficiency of light to heat transduction, we found Sudan IV to be much less effective at driving the decomposition of PPC. In fact, we found degradation of PPC by Sudan IV is nearly 5.5 and 6.5 times less efficient than by gold nanoparticles at the same mass loadings (Table **2-1**). This is despite the fact that these films have larger optical densities at 532 nm than any of the nanoparticle films. We also prepared films of Sudan IV with optical densities at 532 nm equal to the optical densities of the films with [*np*] of 9.9×10^{-3} and 9.9×10^{-2}. Irradiation of these films resulted in mass losses that were statistically no different from those experienced by pure PPC (no nanoparticles). Thus, gold nanoparticles are significantly more efficient than Sudan IV at driving the thermal decomposition of PPC. It seems likely that it is the higher heat capacity of

the nanoparticles that makes them superior sensitizers for driving thermal reactions, though further experiments are needed to confirm this.

Table **2-2**. Polypropylene Carbonate Decomposition (7,000 pulses, 532 nm, 200 mJ/cm^2)

X	*Mass Ratio (X:PPC)*	*% Decomposition*
AuNP	1:10	72 ± 5
	1:100	82 ± 4
Sudan IV	1:10	13 ± 1
	1:100	13 ± 2
PPC	——	3 ± 1

Conclusions

In the above work, we were able to follow the thermal decomposition of a polymer driven by the photothermal effect of 2 nm AuNPs. Collection and characterization of the volatile monomer product allowed us to estimate kinetics as well as temperatures achieved. We found that, at the laser fluencies supplied, AuNPs are capable of reaching minimum temperatures in excess of 800 K in very short periods of time (< 60 μs), and that they are many times more efficient than organic dyes for driving this reaction.

By understanding the temperatures gold nanoparticles are capable of imparting, we can begin to see the potential of applying plasmonic heat not only to common, low temperature reactions, but also to much higher, extreme temperature reactions with little affect to the bulk environment. While it seems to make sense that intense heat can be applied to breaking bonds, using this same heat to form bonds seems less likely. Therefore, in Chapter **3**, we will

demonstrate the ability of plasmonic heat to create bonds, and further establish it as a general synthetic tool capable of driving a variety of reactions in a highly-controlled manner.

References

1. Fasciani, C., Alejo, C. J., Grenier, M., Netto-Ferreira, J. C. & Scaiano, J. C. High-temperature organic reactions at room temperature using plasmon excitation: decomposition of dicumyl peroxide. *Org. Lett.* **13**, 204–207 (2011).
2. Duncan, B., Kim, C. & Rotello, V. M. Gold nanoparticle platforms as drug and biomacromolecule delivery systems. *J. Controlled Release* **148**, 122–127 (2010).
3. Dreaden, E., Alkilany, A., Huang, X., Murphy, C. & El-Sayed, M. The golden age: gold nanoparticles for biomedicine. *Chem. Soc. Rev*. **1**, 2740 (2012).
4. Chen, H. et al. Direct Laser Writing of Microtunnels and Reservoirs on Nanocomposite. *Materials Adv. Mater*. **18**, 2876–2879 (2006).
5. Ueno, K. et al. Nanoparticle Plasmon-Assisted Two-Photon Polymerization Induced by Incoherent Excitation Source. *J. Am. Chem. Soc*. **130**, 6928–6929 (2008).
6. Alessandri, I. & Depero. Laser-induced modification of polymeric beads coated with gold nanoparticles. *Nanotechnology* **19**, 305301 (2008).
7. Ueno, K., Juodkazis, S., Shibuya, T., Mizeikis, V., Yokota, Y. & Misawa, H. Nanoparticle-Enhanced Photopolymerization. *J. Phys. Chem. C* **113**, 11720-11724 (2009).
8. Alessandri, I. Writing, Self-Healing, and Self-Erasing on Conductive Pressure-Sensitive Adhesives. *Small* **6**, 1679-1685 (2010).
9. Alessandri, I., Ferroni, M. & Depero. Plasmon-Assisted, Spatially Resolved Laser Generation of Transition Metal Oxides from Liquid Precursors. *J. Phys. Chem. C* **115**, 5174-5180 (2011).
10. Linic, S., Christopher, P. & Ingram, D. B. Plasmonic-metal nanostructures for efficient conversion of solar to chemical energy. *Nat. Mater*. **10**, 911-921 (2011).
11. Zillohu, A., Abdelaziz, R., Hedayati, M. K., Emmler, T., Homaeigohar, S. & Elbahri, M. Plasmon Mediated Embedding of Nanoparticles in a Polymer Matrix; Nanocomposites Patterning, Writing and Defect Healing. *J. Phys. Chem. C* **116**, 17204-17209 (2012).
12. Huihong, L., Lisha, P., Qiang, L., Nai, X. & Lingbin, L. Preparation and characterization of poly (propylene carbonate)/polystyrene composite films by melt-extrusion method. *e-Polymers*, **10**, 390–398 (2010).
13. Maier, C. & Calafut, T. *Propylene: The Definitive User's Guide and Databook* (Plastics Design Library, Norwich, 1998).
14. Peng, S., An, Y. Chen, C., Fei, B., Zhuang, Y. and Dong, L. Thermal degradation kinetics of uncapped and end-capped poly(propylene carbonate). *Polym. Degrad. Stabil*. **80**, 141-147 (2003).
15. Lu, X. L., Zhu, Q. & Meng, Y. Z. Kinetic analysis of thermal decomposition of poly(propylene carbonate). *Polym. Degrad. Stabil*. **89**, 282-288 (2005).
16. Jain, P. K.; Lee, K. S.; El-Sayed, I. H. & El-Sayed, M. A. Calculated absorption and scattering properties of gold nanoparticles of different size, shape, and composition: applications in biological imaging and biomedicine. *J. Phys. Chem. B* **110**, 7238-7248 (2006).
17. Hu, M. & Hartland, G. V. Heat Dissipation for Au Particles in Aqueous Solution: Relaxation Time versus Size. *J. Phys. Chem. B* **106**, 7029-7033 (2002).
18. Abad, A.; Corma, A. & García, H. Supported gold nanoparticles for aerobic, solventless oxidation of allylic alcohols. *Pure and Applied Chemistry*, **79**, 1847–1854 (2007).
19. Link, S. & El-Sayed, M. A. Shape and Size Dependence of Radiative , Non-Radiative and Photothermal Properties of Gold Nanocrystals. *Int. Rev. Phys. Chem.* **19**, 409-453 (2000).

20. Schmid, Günter. *Clusters and Colloids: From Theory to Applications.* (Weinheim; New York: VCH, 1994).
21. Brust, M., Walker, M., Bethell, D., Schiffrin, D. J. & Whyman, R. Synthesis of thiol-derivatised gold nanoparticles in a two-phase liquid-liquid system. *Chem. Comm.* **7**, 801-802 (1994).
22. Haas, K. M. & Lear, B. J. Degradation of polypropylene carbonate through plasmonic heating. *Nanoscale* **5**, 5247-5251 (2013).
23. Hodak, J. H., Henglein, A. & Hartland, G. V. Photophysics of Nanometer Sized Metal Particles: Electron−Phonon Coupling and Coherent Excitation of Breathing Vibrational Modes.
24. G. F. Bohren and D. R. Huffman. *Absorption and Scattering of Light by Small Particles* (Wiley, New York, 1983).
25. Huttmann, G. & Birngruber, R. On the possibility of high-precision photothermal microeffects and the measurement of fast thermal denaturation of proteins. *IEEE J. Sel. Top. Quant.* **5**, 954-962 (1999).

Appendix for Chapter 2

Using Reaction Kinetics to Determine Photothermal Temperatures

Details of film preparation

Sample films were prepared by dissolving AuNPs and polypropylene carbonate (PPC) in methylene chloride in nanoparticle:PPC mass ratios of 1:10, 25, 50, 75, 100, 250, 500, and 750. The solutions were always made such that the PPC in methylene chloride was at a concentration of 0.2g/ml. The mixtures were micropipetted on to pre-weighed microscope slides in a volume of 40 μL, and allowed to dry for 24 hours. After drying, the slides were again weighed, and then exposed to 7,000 pulses of a frequency-doubled 532 nm Nd:YAG laser (Quanta Ray 130, 8 ns pulses, 10 Hz). After irradiation, the slides were reweighed and the mass loss recorded.

Determination of the extinction coefficient (ε_{532}) of the films

To determine the extinction coefficient present in the films, a solution of nanoparticles and polypropylene carbonate was made, as if to be deposited on slides to form a 1:100::nanoparticle:PPC (by mass) film. Noted was (*i*) the mass of nanoparticles, (*ii*) the mass of PPC, and (*iii*) the volume of methylene chloride. This solution was then diluted until the absorbance maximum at 532 nm was less than 1 absorption unit when using a quartz cuvette with a 1 cm path length. The extinction coefficient for this solution was then calculated and this value (together with the dilution factor) used to calculate the extinction coefficient of the original solution.

Once the extinction coefficient for the original solution was determined, we then determined the extinction coefficient of the films. This was done by assuming that only the methylene chloride would evaporate in the films, leaving behind the nanoparticles and the PPC. This amounts to further concentration of the film. The loss in volume of the methylene chloride was used to calculate the degree of concentration, which in turn was used to give the extinction coefficient of the nanoparticles in the film. Following this procedure we find: $\varepsilon_{532} = 0.641\ mg_{film}\ mg_{nanopartilce}^{-1}\ \mu m^{-1}$.

Due to the heterogeneity inherent in dealing with nanoparticles, we do not report the extinction coefficient in terms of molarity, rather we report it in terms of mass fraction. It is important to note that this means that this extinction coefficient is only viable for the specific nanoparticles (heptane thiol protected) and polymer (PPC) that we use here. Adaptation to other chemical systems could be done, if the relative densities of the nanoparticles and polymers are known.

Description of quantum yield measurements

Quantum yield measurements were made in the laboratory of Prof. Mark Maroncelli with the help of Jens Breffke. Steady-state absorption spectra were measured using a Hitachi U-3010 UV/vis spectrophotometer and corrected emission spectra with a Spex Fluorolog F212 fluorimeter. These instruments have been used to successfully measure quantum yields of 10^{-4}. We observed no detectible fluorescence form Sudan IV and so assume the quantum yield must be less than 0.1. This is sufficient to conclude that the vast majority of the energy absorbed by the dye is converted to heat via a non-radiative pathway and supported our choice of Sudan IV as a valid organic dye for comparison of the photothermal effect with that of gold nanoparticles.

Chapter 3

Constructively Using Photothermal Heat

Introduction

Improving heat as a synthetic tool requires not only control over its spatial and temporal distribution and magnitude, but also the ability to apply it to a variety of transformations. In Chapter **2**, we examined bond breaking through the thermal decomposition of a polymer with high activation barriers. We found that AuNPs are quite strong light absorbers capable of efficiently and rapidly converting light to heat and cleanly breaking bonds, and to do so with unprecedented resolution in both time (picoseconds) and space (nanometers). Plasmonic heat has also been utilized to drive other destructive processes including the melting of solids,[1-3] the boiling of liquids, [4,5] controlled release of molecules from materials,[6-9] and killing of cancerous cells.[10-13] All of these transformations are realized without damage to the surroundings – a result that highlights the fact that these transformations occur at localized 'effective temperatures' that are not realized by the bulk material. This result is particularly intriguing for chemical bond cleavage, as it allows targeted destruction with molecular scale precision.

While the destructive power of the photothermal effect is undeniable, the power of chemical synthesis rests not only on the ability to cleave bonds, but also to form and isomerize bonds. In order for plasmonic heat to be considered an efficient and general heat source capable of replacing current synthetic heating techniques, it becomes important to demonstrate its versatility for chemical transformations beyond bond cleavage.

In many respects, the application of extreme temperatures is ideal for bond cleavage. For example, the triple bonds in N_2 are very strong (ca. 950 kJ/mol), making this molecule relatively inert.[14] However, the homolytic cleavage of N_2 can be accomplished at temperatures in excess of

500°C, demonstrating that for even the strongest bonds, a temperature can be identified that allows escape from its potential energy well.[15] While breaking bonds simply requires escape from the potential well, a feat that can be accomplished with enough energy, occupation of potential energy wells, as required by constructive events (i.e. bond formation), rely on more precise application of thermal energy – enough to overcome the reaction barrier, but not enough to destroy the products. While previous applications of the photothermal effect indicate that it may not be useful for these events, the rapid cooling of the particles provides a possible means for trapping of species transiently generated at high temperatures before they escape the energy well. Below, we demonstrate the ability of the photothermal effect of AuNPs to drive bond formation between isocyanates and alcohols, yielding urethane moieties with unprecedented rates of reaction.

Choosing a Model System for Bond Formation

Our work focuses on the polymerization of polyurethane films from hexamethylene diisocyanate (HDI – formulated as Desmodur N3600), and the diester polyol poly-bis(triethylol) heptanedioate (BTEH – formulated as K-FLEX 188) (Scheme **3-1**). For a number of reasons, this transformation is an ideal bond formation. First, the formation of urethane is spontaneous at room temperature, and this provides a baseline rate of bond formation to which we can compare the impact of photothermal heating.[16,17] Second, there are many known chemical catalysts for this reaction – the most common being dibutyltin dilaurate (DBTDL) – to which we can also compare the efficacy of the photothermal effect.[18,19] Third, the urethane bond is relatively weak (100-130 kJ/mol), and can be cleaved at temperatures (125 °C to 250 °C) far below the peak temperatures produced by the photothermal effect of gold nanoparticles (which can reach thousands of degrees).[20-22] Thus, if net bond formation is observed, it must occur through the thermal quenching described above. Fourth, given reasonable estimations for the enthalpic (-132 kJ/mol)

and entropic (-188 J/mol) changes associated with urethane formation, the equilibrium for this reaction should lie far to the reactants at the extreme temperatures (K_{800K} = 6.63 x 10^{-2} M^{-1}) our conditions are known to produce.[23] Thus, significant progress of the reaction can only be ascribed to trapping of transiently formed products during thermal quenching – rather than simple biasing of the equilibrium at high temperatures. Finally, the facile ability to produce polyurethanes with rigid or flexible forms allows them to be widely employed in a variety of applications. For example, they can be used as short-term surgical implants, light-weight foams in cars, and fine threads in garments.[24-26] The ability to use urethanes for on-demand applications would greatly extend the physical and chemical properties obtainable in such applications and the work described below provides the basis for on-demand thermal curing of urethane polymer films.

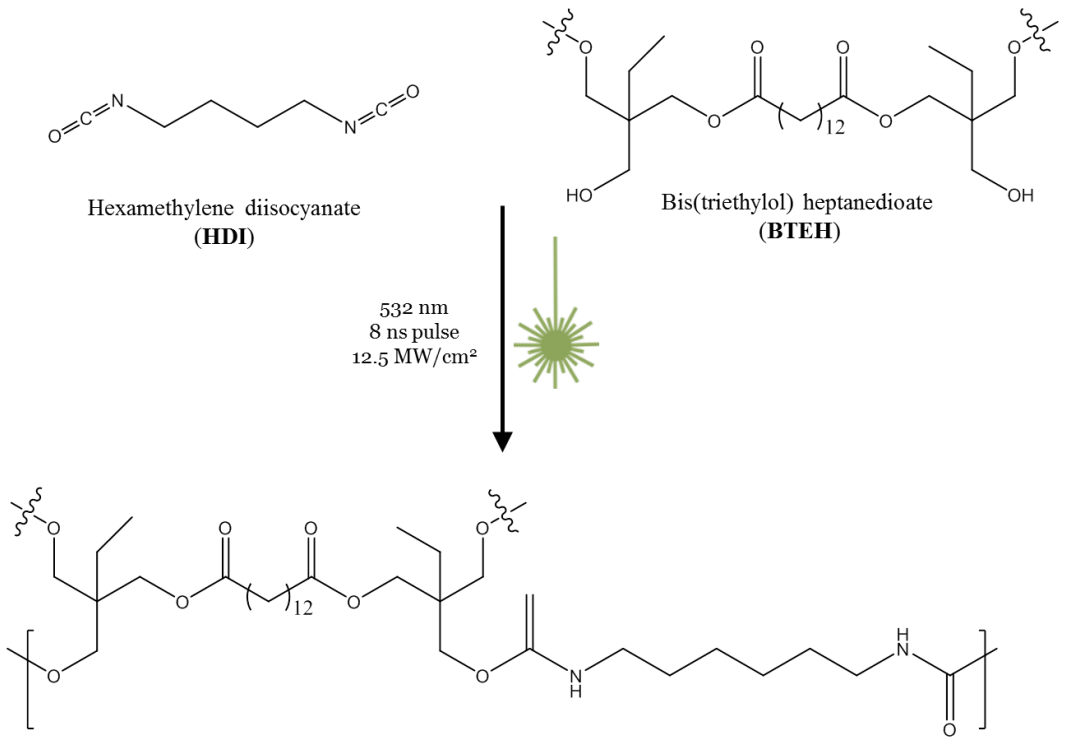

Scheme **3-1**. Urethane formation reaction between hexamethylene diisocyanate (HDI) and diester polyol poly-bis(triethylol) heptanedioate (BTEH).

In addition to the kinetic, energetic, and practical considerations outlined above, the progress of urethane polymerization can be followed via several excellent infrared (IR) markers. Figure **3-1a** shows the evolution of the IR spectrum during the reaction between HDI and BTEH (in equal parts alcohol:isocyanate moieties) at room temperature. The most obvious change in the spectrum is the loss of intensity in the isocyanate stretching mode (2274 cm^{-1}) (Figure **3-1a)**. However, several other changes are also present. Though small, the intensity of the free OH stretch (3550 cm^{-1}) also diminishes during the course of the reaction. Concomitantly, a band associated with C—O—C stretching mode of the urethane (1242 cm^{-1}) appears. The rate of disappearance of the isocyanate and alcohol modes are mirrored by the growth of the C—O—C mode (Figure **3-1b**) – confirming that these features of the IR spectra are reporting on the conversion of isocyanate and alcohols into urethane. Given the fact that the isocyanate mode presents the most isolated band, we choose this as our primary reporter on kinetics as we moved on to study the efficacy of the photothermal effect for driving urethane formation.

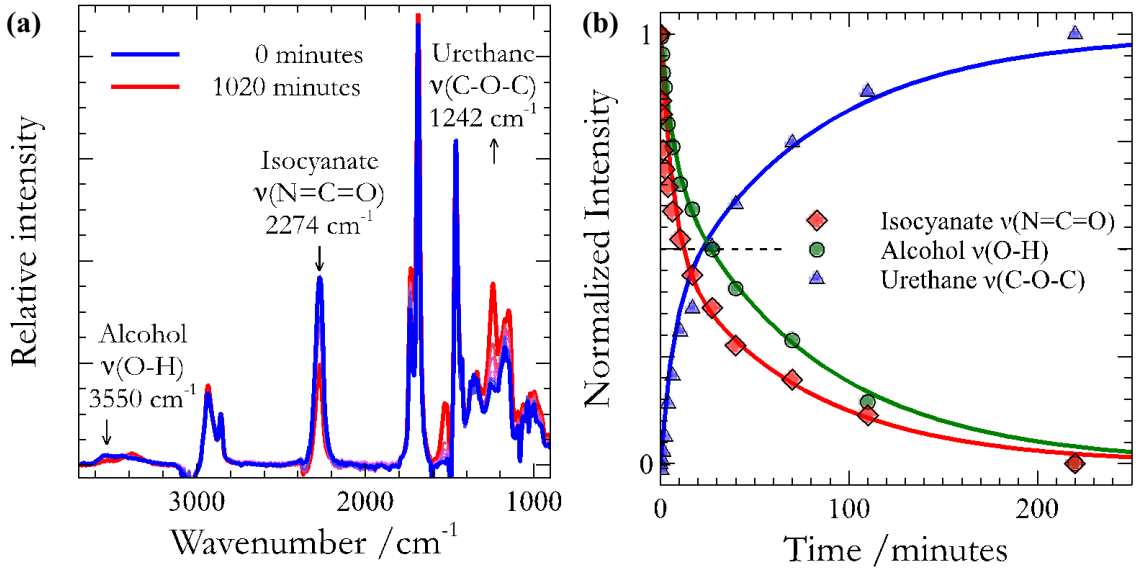

Figure **3-1**. The reaction between HDI and BTEH to form polyurethane followed using (a) infrared spectroscopy. In particular, we observe the loss of bands associated with the isocyanate (2274 cm^{-1}) and alcohol (3550 cm^{-1}) moieties, and the appearance of the C-O-C mode (1242 cm^{-1}) associated with the urethane. (b) The kinetics associated with these changes indicate direct conversion to urethane.

The heart of our study is a comparison between the impact of the photothermal effect upon the rate of catalyzed and un-catalyzed urethane polymerization. In order to isolate the effect of light upon these conditions, we investigated the curing rate of urethane (Scheme **3-1**) under all combinations of AuNPs, DBTDL, and light (Figure **3-2**, Table **3-1**). For this study, we worked with octanethiol-protected AuNPs with diameters of ~2 nm. These particles are near the smallest that support a SPR (Appendix), and thus have the desired photophysical properties that lead to the photothermal effect. Though larger particles would possess a stronger SPR (and associated photothermal effect), we chose to use small particles for the kinetics of thermal diffusion. The smaller the particle, the faster the quenching of the temperatures, and the more likely we are to trap transiently formed chemical bonds. For 2 nm AuNPs, the decay of the temperature is on the order of 10 ps,[4] and can compete with the kinetics of bond formation/cleavage. Thus, for our first demonstration of the constructive use of the photothermal effect, we favored kinetic considerations over strength of the photothermal effect.

Experimental

A full, detailed description of the experimental procedures can be found in the Appendix. Briefly, the appropriate solutions were made by mixing HDI and BTEH in an approximately 1:1 ratio with either pure toluene, or toluene solutions containing either AuNPs or DBTDL, or both. In all cases containing AuNPs or DBTDL, the final concentrations of these additives were 0.08% w/v and 0.07% w/v, respectively. These concentrations were chosen based upon preliminary data, such that the action of the photothermal effect would be comparable to the action of the catalyst. The final concentration of isocyanate was 13.7 M, which is similar to that used in industrial applications of urethane films.

Once the solutions were prepared, the reaction between HDI and BTEH was allowed to proceed for four minutes, either in the presence or absence of light. For those exposed to light, we

used 8 ns pulses (50 mJ per pulse) of 532 nm light from a QuantaRay 130 Nd:YAG laser operating at a repetition rate of 10 Hz. The peak irradiance for these pulses is 12.5 MW cm^{-2}. The polymerization of isocyanate and polyol to polyurethane was monitored following the disappearance of the free isocyanate peak at 2274 cm^{-1}.

Urethane Polymerization Kinetics

Figure **3-2** shows the kinetic traces obtained from the isocyanate band in the IR under all eight permutations. In all cases, we found that the early time kinetics (up to 4 minutes) were reasonably linear (χ^2 better than 0.84) and so we also show the results of linear regressions to the data. At long times, the kinetics deviated strongly from linearity (Figure **3-1b**), as one might expect for the second order kinetics that underlie polyurethane curing.[22,23] However, it is interesting that for the fastest observed reaction, the reaction kinetics remain linear up to ca. 50% conversion. We did not anticipate this result, which maintains a linear response much closer to reaction completion than the kinetics observed for the pure polymer. This unusual action by the photothermal effect may be an additional consequence of the localized nature of the heat, which allows the reaction to run to near completion near the surface of the nanoparticle. Diffusion of the particle between pulses of the laser would allow the particle to enter a region of unreacted isocyanate and alcohol, where the process would repeat. Though speculative, this would provide a mechanism for the observed linearity up to 50% completion under action of AuNPs, DBTDL, and light (condition viii).

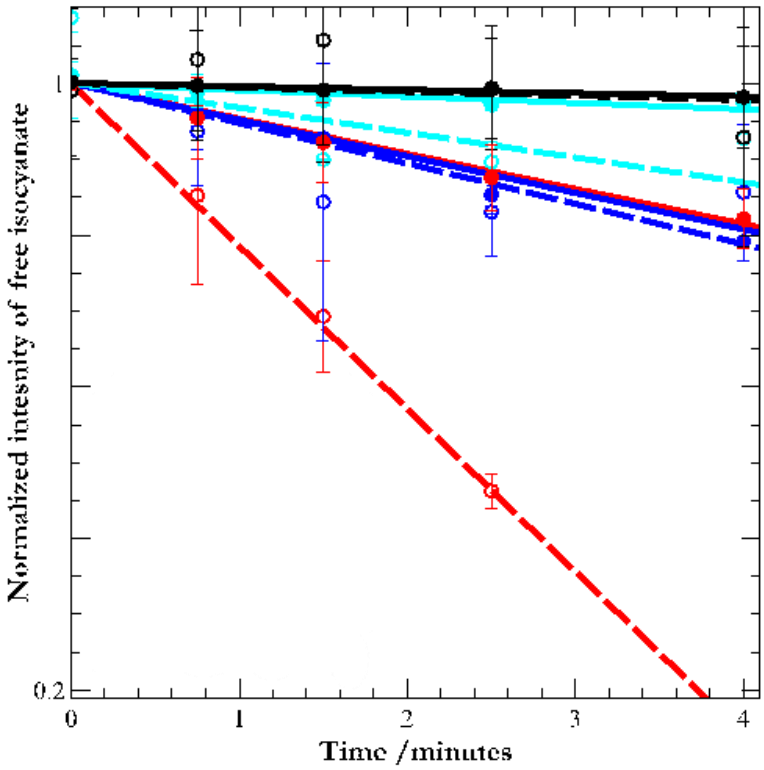

Figure **3-2**. Kinetic traces following the disappearance of the isocyanate band (2274 cm-1)

		CONDITIONS		
		AuNP	**Catalyst**	**Light**
(i)	●—●	—	—	—
(ii)	●···○···●	—	—	✓
(iii)	●—●	✓	—	—
(iv)	●···○···●	✓	—	✓
(v)	●—●	—	✓	—
(vi)	●···○···●	—	✓	✓
(vii)	●—●	✓	✓	—
(viii)	●···○···●	✓	✓	✓

Table **3-1**. The eight combinations of AuNP, catalyst, and light.

Enhancement of Polymerization Rate

Given that all conditions gave rise to linear early kinetics, we chose to focus on these kinetics, and our comparisons between the various conditions are in terms of the initial rates of reaction. Using these rates, which we determined from the slopes shown in Figure **3-2**, we next calculated the relative enhancement of bond formation for each condition, by dividing the rate for each condition by the rate of the pure polymer film in the dark (condition i). The enhancement factors are shown in Figure **3-3** and Table **3-2**.

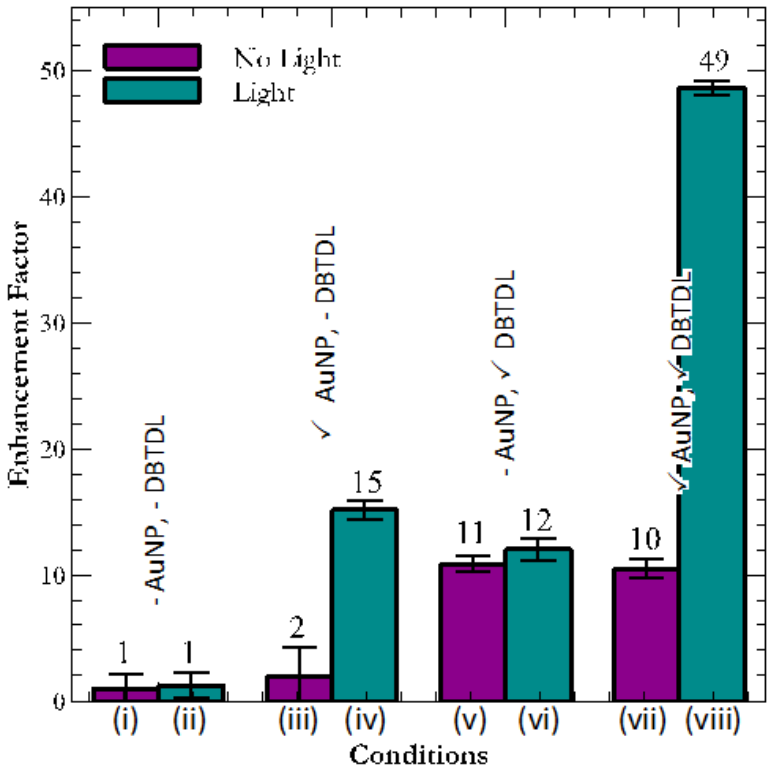

Figure **3-3**. The relative rate of reaction (with respect to pure polymer) for all eight conditions.

Table **3-2**. Summary of enhancements, observed temperature changes, and anticipated temperature changes for all eight conditions. We show the results calculated for real time and irradiated time.

Condition			Enhancement	ΔT_{abs}	$\Delta T_{kinetics}$
Real Time					
HDI + BTEH	*i*	No Light	1	0	0
	ii	Light	1	0	0
HDI + BTEH + AuNP	*iii*	No Light	2	0	0
	iv	Light	15	12	65
HDI + BTEH + DBTDL	*v*	No Light	11	0	0
	vi	Light	12	0	0
HDI + BTEH + AuNP + DBTDL	*vii*	No Light	10	0	0
	viii	Light	49	8	65
Irradiated Time					
HDI + BTEH + AuNP	*iv*	Light	$1.55 \times 10^{+09}$	12	305
HDI + BTEH + AuNP + DBTDL	*viii*	Light	$4.8 \times 10^{+09}$	8	322

There are a number of interesting results that are apparent from inspection of Figure **3-3** and Table **3-2**. To begin, only samples containing AuNPs experience rate enhancement upon exposure to light. These results imply that the AuNPs are the only significant source of photothermal heating – an important result given that DBTDL is a slightly colored compound (see Appendix for UV-Vis). It also implies that any increase in reaction rate upon exposure to light must stem from the action of AuNPs.

In addition, the photothermal enhancement for films with only AuNPs is comparable to the rate enhancement for films with only catalysts, which means that the photothermal effect of AuNPs competes on a weight-by-weight basis with the action of traditional catalysts. However, we can also consider the action on a per-number basis. The relative mass difference between the catalytic molecules (631.56 g/mol) and the AuNPs (~ 4.9×10^4 g/mol) implies that, on a per-number basis, the photothermal effect of gold is approximately 90 times more efficient at accomplishing urethane formation than is the catalytic effect of DBTDL. Here it is important to realize that the molecular mass given for AuNPs is only a rough estimate based upon the mean

size of a polydisperse sample. The greater effectiveness per AuNP was an anticipated result, as the AuNP is able to create an area effect, while the catalyst interacts on a one-to-one basis with its substrate.

Photothermal Effects on Polymerization Rate

There is also a synergistic effect between the action of the DBTDL and the photothermal effect of the gold nanoparticles. That is, the enhancement of the rate is not the simple addition of the enhancements for DBTDL and AuNPs alone. Importantly, without light, the samples with DBTDL alone and DBTDL+AuNPs experience the same rate – meaning that the presence of AuNPs is not sufficient for this synergy; instead the SPR of the AuNP must be excited. In addition, irradiation of DBTDL produces no enhancement relative to the action of DBTDL alone. Thus, the large synergy must result from the excitation of the AuNPs' SPR in the presence of DBTDL. This conclusion implies that there is some interaction between DBTDL and the AuNPs, during irradiation, though the exact nature of this interaction in not clear at this time. Possible sources of synergy could be increased mobility of the liquid components, which would facilitate the diffusion-limited action of the catalyst. In addition, it is known that HDI exists (in part) as a trimer, joined at the isocyanate moieties.[27] This trimer can be broken at high temperatures, and increases the concentration of free isocyanates. Thus, if the photothermal effect results in the breaking of the trimer, this would make more free isocyanates available to react with the alcohols and DBTDL in solution – providing another mechanism for the observed synergy.

In order to ensure that the rate enhancements observed for the photothermal effect were not merely a result of bulk-scale temperature increases, we measured the temperature changes during the course of the reaction under all eight conditions. This was done using an IR thermal imager (Raytek ThermoView Ti30) to acquire temperature measurements before and after 4 minutes, for the same conditions used to generate Table **3-1**. A summary of the observed

temperature changes (ΔT_{obs}) are given in Table **3-2**. As can be seen, the only conditions that led to an observable temperature increase were those in which AuNPs were exposed to laser light. However, in these cases, the bulk-temperature jump was far too small (on the order of 10 K) to account for the observed rate increases. We confirmed this last point by following the kinetics of polymer formation under several temperatures, attained by bulk heating in an oil bath (Appendix). These results indicate that we would need bulk temperatures changes ($\Delta T_{kinetics}$) of ca. 65 K in order to observe the kinetic enhancement achieved by the photothermally driven reactions. Thus, the observed photothermal enhancement is not an effect of simple bulk-scale heating, but the result of transient and intense heat produced near the AuNPs' surface.

The above conclusion – that it is the localized and transient heat that gives rise to the rate enhancement – carries with it several additional implications. First, this implies that the reaction rate is only increased while the AuNP is hot. Given the fast rise and decay of the temperature for these particles, we can approximate that the particles are only hot for the duration of the laser pulse (8 ns) – or a total of ca. 20 μs during the course of our 4 minute experiments.[28] If we recalculate the rate of reaction using the total irradiation time (Table **3-2**), we arrive at an astonishing enhancement of reaction rate on the order of billion-fold (Figure **3-4**). However, this may still be an underestimate of the rate enhancement. Since the heating and cooling of a nanoparticle occurs within ~10 ps, and the heat initially generated upon irradiation is intense, an 8 ns pulse is quite long compared to this photophysical event and will behave more like continuous irradiation. Over the course of this pulse, the heat delivered to the surroundings will be limited by the thermal diffusivity of the surrounding environment, and therefore be much lower beyond the initial heat delivery.

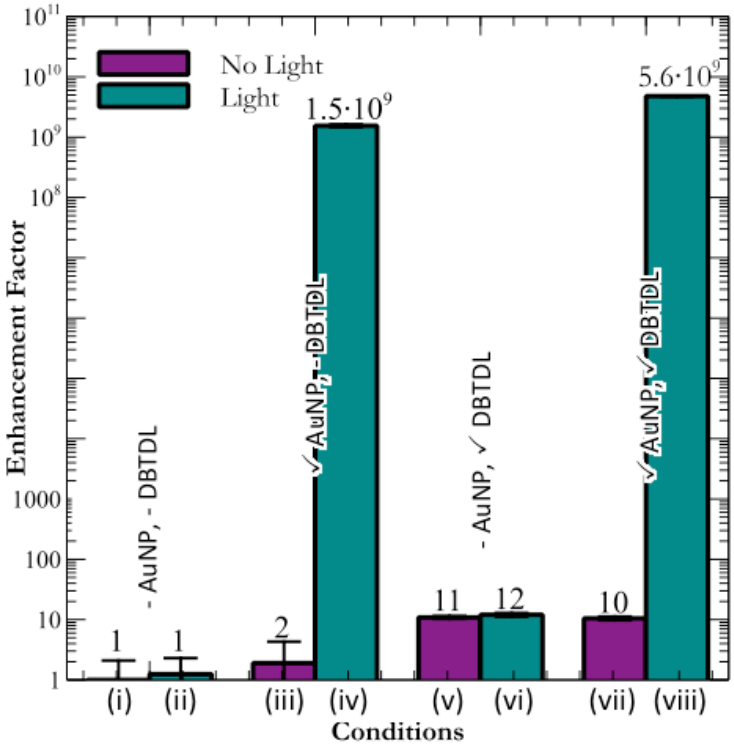

Figure **3-4**. The relative rate of reaction (with respect to pure polymer) for all eight conditions calculated using the total irradiation time of 20 μs for samples experiencing photothermal heating.

The rate adjusted for irradiation time further implies a temperature of at least 600 K – though the actual temperature near the nanoparticle surface must be many times higher. Again, given the energetics of this reaction, the equilibrium should lie far to the side of the reactants at these temperatures and so the observed completion percentage must result from the trapping of transiently formed bonds during the thermal quenching of the particles. This conclusion highlights the unique ability of the photothermal effect to quickly drive bond formation at 'effective' temperatures that are far higher than those that would otherwise fail to give rise to appreciable reaction progress.

The fact that light can be used to accomplish these remarkable feats further emphasizes the benefits of photothermal heating over traditional catalysts, such as DBTDL. Unlike traditional catalysts, the efficiency of the AuNPs should be easily and dynamically tunable via

alteration of the conditions. Indeed, increasing either the irradiance or the repetition rate of the laser should give rise to an increase in the efficacy of the photothermal effect. Simple consideration of the timescales associated with the photothermal effect suggests a further million-fold increase in repetition rate could be applied, while still realizing gains in efficacy. Thus, use of the photothermal effect provides the possibility of dynamic tuning of the reaction rate over 12 orders of magnitude – though future work will be required to experimentally verify this remarkable prediction.

Conclusions

In conclusion, we have used urethane formation to demonstrate the first use of photothermal heating for efficiently and effectively driving bond formation on the bulk scale. The bulk scale transformations are surprising given the fact that the heat produced is localized to the nanometer scale. In real time, we observe significant (50x) enhancement of the rate of urethane formation. In addition, we have shown that these enhancements stem not from bulk-scale heating, but from the localized and intense heat that the nanoparticles provide. With this knowledge, we are able to show that the photothermal enhancement is closer to a billion-fold increase, with the ability to realize a million fold more.

Thus far, we have demonstrated the ability of plasmonic heat to be applied to a variety of transformations, both constructive and destructive, and that we are able to achieve high temperatures in an on-demand fashion. This work is an important step in developing the photothermal effect as a well-controlled heating method. While the work represented in this dissertation utilizes AuNPs as photothermal agents, these particles possess some disadvantages that may prevent the photothermal effect from wider application. In Chapter **4**, we address the drawbacks of using gold and explore alternative photothermal agents.

References

1. Richardson, H. H. et al. Thermooptical properties of gold nanoparticles embedded in ice: characterization of heat generation and melting. *Nano Lett.* **6**, 783-8 (2006).
2. Zillohu, A. U.; Abdelaziz, R.; Hedayati, M. K.; Emmler, T.; Homaeigohar, S. & Elbahri, M. Plasmon Mediated Embedding of Nanoparticles in a Polymer Matrix; Nanocomposites Patterning, Writing and Defect Healing. *J. Phys. Chem. C* **116**, 17204-17209 (2012).
3. Maity, S., Downen, L. N., Bochinski, J. R. & Clarke, L. I. Embedded metal nanoparticles as localized heat sources: An alternative processing approach for complex polymeric materials. *Polymer* **52**, 1674-1685 (2011).
4. Jones, C. D.; Lyon, L. A. Photothermal patterning of microgel/gold nanoparticle composite colloidal crystals. *J. Amer. Chem. Soc.* 125, 460-465 (2003).
5. Fang, Z.; Zhen, Y.-R.; Neumann, O.; Polman, A.; García De Abajo, F. J.; Nordlander, P. & Halas, N. J. Evolution of Light-Induced Vapor Generation at a Liquid-Immersed Metallic Nanoparticle. *Nano Lett.* **13**, 1736-1742 (2013).
6. Poon, L.; Zandberg, W.; Hsiao, D.; Erno, Z.; Sen, D.; Gates, B. D. & Branda, N. R. Photothermal release of single-stranded DNA from the surface of gold nanoparticles through controlled denaturating and Au-S bond breaking. *ACS Nano* **4**, 6395-403 (2010).
7. Asadirad, A. M., Erno, Z. & Branda, N. R. Photothermal release of singlet oxygen from gold nanoparticles. *Chem. Comm.* **49**, 5639 (2013).
8. Estrada, A. C.; Daniel-da-Silva, A. & Trindade, T. Photothermally enhanced drug release by kappa-carrageenan hydrogels reinforced with multi-walled carbon nanotubes. *RSC Adv.* **3**, 10828-10836 (2013).
9. Nguyen, D. T.; Truong, R.; Lee, R.; Goetz, S. A.& Esser-Kahn, A. P. Photothermal release of CO2 from capture solutions using nanoparticles. *Energy Environ. Sci.* **7**, 2603-2607 (2014).
10. Huang, X., El-Sayed, I. H., Qian, W. & El-Sayed, M. A. Cancer cell imaging and photothermal therapy in the near-infrared region by using gold nanorods. *J. Amer. Chem. Soc.* **128**, 2115-20 (2006).
11. El-Sayed, I. H., Huang, X. & El-Sayed, M. A. Selective laser photo-thermal therapy of epithelial carcinoma using anti-EGFR antibody conjugated gold nanoparticles. *Cancer Lett.* **239**, 129-35 (2006).
12. Zharov, V. P.; Mercer, K. E.; Galitovskaya, E. N. & Smeltzer, M. S. Photothermal nanotherapeutics and nanodiagnostics for selective killing of bacteria targeted with gold nanoparticles. *Biophysical Journal* **90**, 619-627 (2006).
13. Cheng, L.; Yang, K.; Li, Y.; Chen, J.; Wang, C.; Shao, M.; Lee, S.-T. & Liu, Z. Facile Preparation of Multifunctional Upconversion Nanoprobes for Multimodal Imaging and Dual-Targeted Photothermal Therapy. *Angew. Chem. Int. Edit.* **50**, 7385-7390 (2011).
14. Petrucci, R.H.; Harwood, W.S.; Herring, F.G. & Madura, J.D. *General Chemistry Principles and Modern Applications, 9th Ed.* (Pearson Prentice Hall, Upper Saddle River, 2007).
15. Botte, G. G. Electrolytic cells and methods for the production of ammonia and hydrogen. U.S. Patent US8303781 B2, November 6, 2012.
16. Sato, M. Studies on 1-alkenyl isocyanates and their derivatives. *J. Org. Chem.* **26**, 770-779 (1961).
17. Sato, M. Rate of reaction of isycyantes with alcohols. II. *J. Org. Chem.* **27**, 819-825 (1962).
18. Frisch, K. C. & Rumao, L. P. Effect of isocyanate variation on physical and environmental properties of moisture-cure urethan coatings. *J. Paint Tech.* **5**, 461 (1970).

19. Han, Q. & Urban, M. W. Kinetics and mechanisms of catalyzed and noncatalyzed reactions of OH and NCO in acrylic polyol-1,6-hexamethylene diisocyanate (HDI) polyurethanes. VI. *J. Appl. Polym. Sci.* **86**, 2322-2329 (2002).
20. Chattopadhyay, D. K.; Webster, D. C. Thermal stability and flame retardancy of polyurethanes. *Prog. Polym. Sci.* **42**, 1068-1133 (2009).
21. Hentschel, T.; Munstedt, H. Kinetics of the molar mass decrease in a polyurethane melt: a rheological study. *Polymer* **42**, 31953203 (2001).
22. Nedyalkov, N. N.; Imamova, S. E.; Atanasov, P. A.; Toshkova, R. A.; Gardeva, E. G.; Yossifova, L. S.; Alexandrov, M. T. & Obara, M. Interaction of gold nanoparticles with nanosecond laser pulses: Nanoparticle heating. *Appl. Surf. Sci.* **257**, 5456-5459 (2011).
23. Samuilov, A. Y.; Zenitova, L. A.; Bakirova, I. N. & Samuilov, Y. D. Thermodynamic parameters of urethane formation reactions and concomitant processes. *Russ. J. Appl. Chem.* **81**, 1419 (2008).
24. Zdrahala, R.J. & Zdrahala, I.J. Biomedical Applications of Polyurethanes: A Review of Past Promises, Present Realities, and a Vibrant Future. *J. Biomater. Appl.* **14**, 67-90 (1999).
25. Dahlke, B.; Larbig, H.; Scherzer, H.D. & Poltrock, R. Natural Fiber Reinforced Foams Based on Renewable Resources for Automotive Interior Applications. *J. Cell. Plastics* **34**, 361-379 (1998).
26. Krishnan, S. Waterproof breathable fabric laminates and method for producing same. U.S. Patent US5283112 A, February 1, 1994.
27. Boutin, M.; Lesage, J.; Ostiguy, C.; Pauluhn, J. & Bertrand, M.J. Identification of the isocyanates generated during the thermal degradation of a polyurethane car paint. *J. Anal. Appl. Pyrolysis* **71**, 791-802 (2004).
28. Hartland, G. V. Optical studies of dynamics in noble metal nanostructures. *Chem. Rev.* **111**, 3858-3887 (2011).

Appendix for Chapter 3

Constructively Using Photothermal Heat

Synthetic Details

Synthesis and characterization of gold nanoparticle

Gold nanoparticles (AuNPs) were synthesized using the Brust 2-phase method,[1] in which 80 ml of a 0.05 M solution of tetraoctylammonium bromide in toluene was mixed with 30 ml of a 0.03 M solution of hydrogen tetrachloroaurate. Once the gold was transferred to the organic layer, the organic layer was then separated, and 0.84 mmol 1-octanethiol was added to the solution. Then, 25 ml of 0.4 M $NaBH_4$ (aq) was added dropwise, and the mixture was stirred for 3 hours. The organic layer containing gold nanoparticles was purified by precipitation with methanol at 0°C overnight. Figure **3A-1** shows the UV-Vis of the resulting particles, and Figure **3A-2** shows TEM images. The mean diameter of particles before irradiation is 2.1 ± 0.5 nm.

Also shown in Figures **3A-1** and **3A-2** (respectively) are the spectra and TEMs of the AuNPs after irradiation. As can be seen, the particles undergo a change in size during irradiation, growing to give a mean diameter of 4.8 ± 5.1 nm. This growth, which appears to be accomplished by the aggregation of smaller nanoparticles, is not complete and we observe both large and small particles within our samples. The presence of the larger particles gives rise to the stronger plasmonic feature shown in Figure **3A-1**.

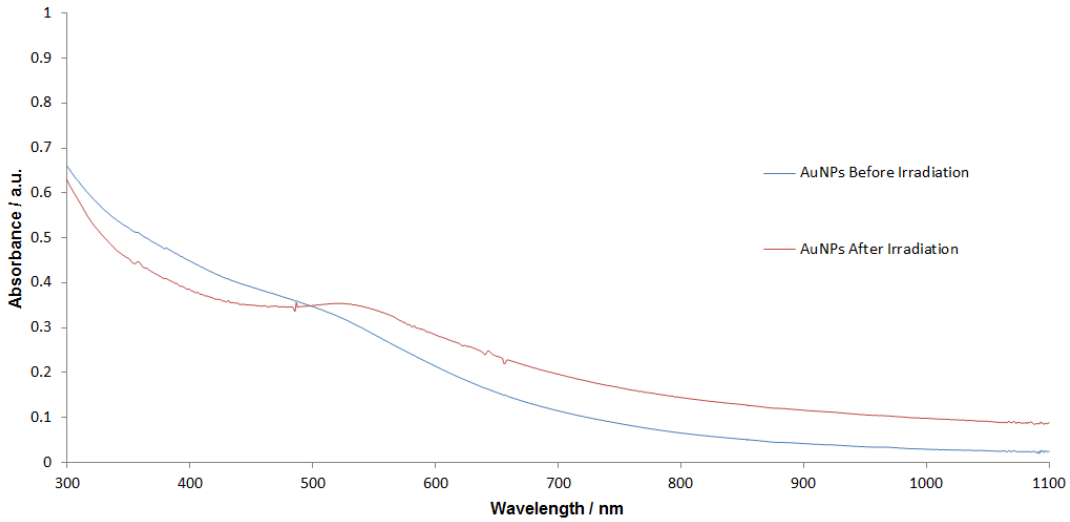

Figure 3A-1. UV-Vis spectrum of AuNPs before and after irradiation

(a) (b)

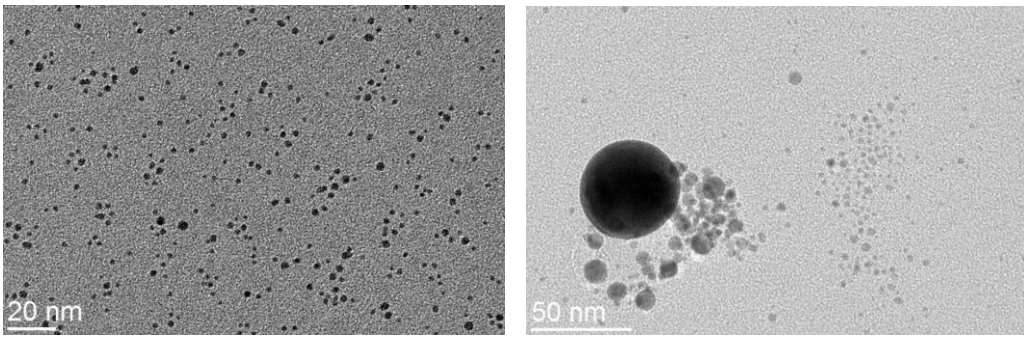

Figure 3A-2. TEM of AuNPs (a) before and (b) after irradiation.

Experimental details of polyurethane film formation

We prepared separate toluene solutions of (a) hexamethylene diisocyanate (HDI – formulated as Desmodur N3600) and (b) the diester polyol bis(triethylol) heptanedioate (BTEH – formulated as K-FLEX 188) prepared so as to maintain a 0.2 g per ml of toluene mass to volume ratio. AuNPs and/or DBTDL (final concentration 0.08% w/v and 0.07% w/v, respectively) were incorporated into the HDI solutions by dissolution in the toluene used to form the solution.

Polyurethane films were then produced by mixing 0.02 ml of each of the above solutions in a culture tube. Samples were either exposed to periods of irradiation by 532 nm light from QuantaRay 130 Nd:YAG laser (8 ns pulses, 10 Hz) or allowed to proceed under ambient conditions. Spectra were collected over a period of 4 minutes, and the disappearance of the isocyanate peak at 2274 cm^{-1} was monitored. IR spectra were collected using a Perkin Elmer Spectrum 400 FT-IR/FT-NIR spectrometer with a Pike Miracle ATR attachment.

Characterization of DBTDL

Dibutyltin dilaurate (DBTDL) was incorporated into appropriate HDI solutions at a loading of 0.07% m/v. UV-Vis characterization is presented in Figure **3A-3**. At the concentrations we used there is very little absorption at 532 nm.

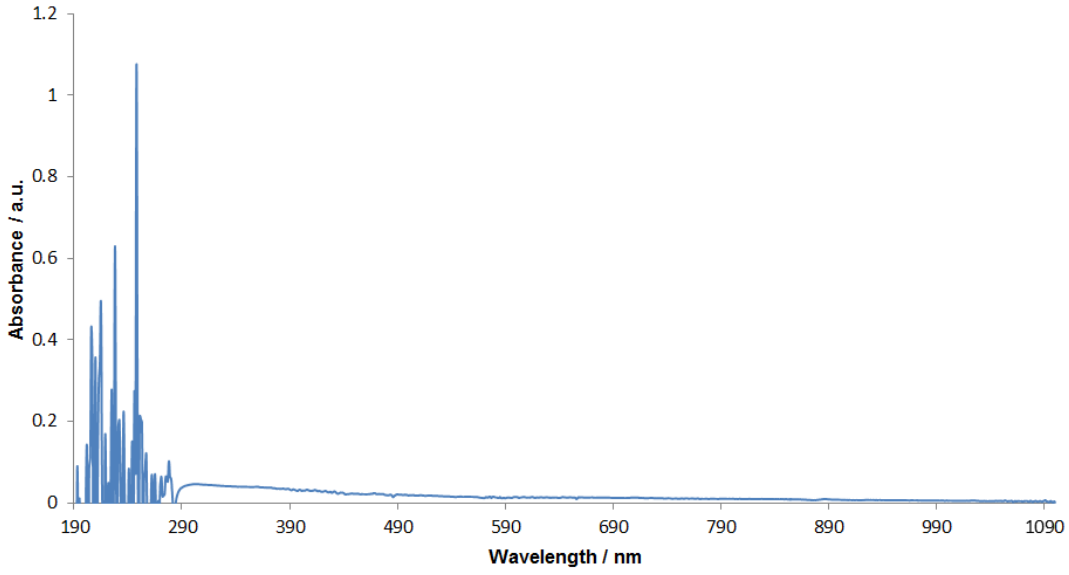

Figure 3A-3. UV-Vis spectrum of 0.07% w/v solution of DBTDL in toluene.

Temperature calibration of polyurethane film formation

In order to determine the impact of bulk-scale heating, we followed the course of the reaction between HDI and BTEH in vials immersed in oil baths held at 50 °C, 75 °C, and 100 °C. The reaction was followed using the same infrared markers as described above and in the manuscript. For each temperature, we fit the early time kinetics and used the slopes to calculate the enhancement of the reaction rate, with respect to that at room temperature (25 °C). This gives us an understanding of the kinetic impact of bulk heating and plotting these data (Figure **3A-4**) allows us to estimate the temperatures that would be required to obtain the kinetic enhancements realized by the photothermal effect (Table **3-2** in Chapter **3**).

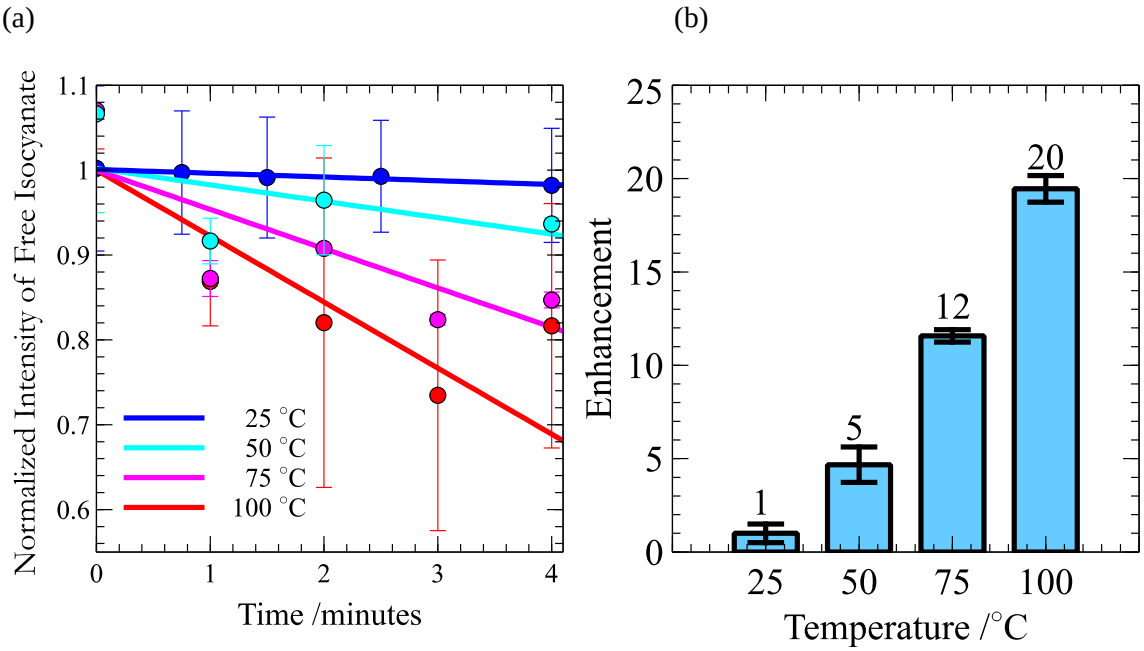

Figure 3A-4. (a) Early time kinetics of polyurethane film formation over time at various temperatures. (b) The enhancement of the kinetics at these temperatures, relative to the room temperature rate.

References

1. Brust, M., Walker, M., Bethell, D., Schiffrin, D. J. & Whyman, R. *Chem. Comm.* **7**, 801-802 (1994).

Chapter 4

The Problem with Gold

Using the photothermal effect to drive chemical transformations is a promising alternative to current heating methods. Where current heating methods require bulk heating to drive molecular transformations, the photothermal effect delivers sufficient heat at the molecular scale, thereby driving reactions with increased efficiency and specificity. My results thus far illustrate the ability of this heat to both cleave (Chapter **2**) and form (Chapter **3**) bonds with molecular level precision while maintaining relatively low bulk temperatures. Furthermore, these transformations are accomplished over a time period of minutes with relatively quick rates of completion when compared to current bulk reactions.

At its heart, the photothermal effect relies on the ability of a species to efficiently absorb light and convert this energy to heat. In most cases, the absorption of light excites electrons that can then relax via radiative and nonradiative pathways, and in order to most efficiently produce heat, nonradiative pathways should dominate. Therefore, it is important to minimize radiative pathways, such as luminescence, so that nonradiative decay may be maximized, making heat production more efficient. Thus, the guidelines for choosing a photothermal agent are simple: strong absorption and weak emission. However, additional requirements, such as stability, may be desirable. Below, I review classes of potential photothermal agents and discuss their advantages and disadvantages.

Agents We Have Examined

Organic Dyes

There are many organic dyes that are strongly absorbing and weakly emitting, suggesting that they will produce high temperatures under irradiation.[1,2] Their small molecular size allows for incorporation into more confined areas, and their synthetic flexibility offers advantages for application, such as the ability for fine tuning (down to the atom) of light absorption and solubility.[3]

In Chapter **1**, we tested the ability of Sudan IV, a strongly absorbing and low luminescing dye, to decompose PPC. We incorporated this dye into PPC and irradiated the films, and we found that at similar mass loadings, Sudan IV showed decomposition significantly lower than films containing AuNPs (Table **2-2**). The small size of organic dyes translates to small absorption cross-sections, capable of only absorbing 1-2 photons per molecule.[4] Organic dyes also have low heat capacities, meaning they will

The small amount of light that organic dyes can absorb paired with their low heat capacity (compared to AuNPs) results in lower achievable temperatures.

In irradiated films containing Sudan IV, we also observed a color change from red to white. This color change is indicative of photobleaching, which decreases the light absorption and therefore heat producing properties of the dye. These are problems that other organic dyes will probably possess as well. It is evident that organic dyes' absorption cross sections are too small to absorb significant amounts of light that can be converted into meaningful heat capable of driving chemical transformations. Furthermore, their tendency to quickly photobleach removes any long term stability of these dyes, rendering them poor photothermal agents.[1,2] Therefore, in addition to requiring strong absorbance and low emission, a photothermal agent must also exhibit

a large absorption cross section, effective heat delivery to the surroundings, and stability under irradiation.

Gold Nanoparticles

Gold nanoparticles are one of the most widely utilized photothermal agents today. They exhibit extinction coefficients 3-4 times greater than that of typical organic dyes, and can absorb multiple photons per particle.[5] These characteristics combined with a large thermal mass allow AuNPs to reach temperatures in excess of 1000 K.[6] In addition to exhibiting large absorption cross-sections and low quantum yields for luminescence, advances in synthetic techniques offer the ability to tailor particle absorption to a variety of applications. AuNPs can be reliably synthesized in a variety of sizes (2 – 100 nm) and shapes (sphere, rod, pyramid) with various absorptions extending from the visible to the NIR region of the electromagnetic spectrum.[7,8] The surface of AuNPs can also be easily modified, which is important for incorporation into a variety of solvent and substrate environments.

Controlling these properties not only opens doors to a variety of applications, but it also offers a means by which to control the SPR exhibited by AuNPs. The SPR depends upon nanoparticle shape and size – properties which can be synthetically controlled – and as illustrated in Scheme **1-1**, SPR excitation and coupling with the phonon is responsible for absorbing and converting light to heat. Therefore, by altering the size and shape of a particle, we can not only decide where the particle will absorb light in the electromagnetic spectrum, but we can also predict how much of this light will be absorbed and converted to heat.

While we have shown that very low concentrations of AuNPs ($\leq$ 0.10% w/v) are capable of efficiently driving chemical reactions, there are some shortcomings to using AuNPs as light-to-heat transducers. Perhaps the most obvious obstacle of using gold is cost of the synthetic materials. Currently valued at $38,000 per kilogram, gold is one of the most expensive metals in

the world, which directly translates to a costly gold salt precursor.[9] If we return to the example of curing thin films on cars that was introduced in Chapter **1**, the cost of the materials to create a 0.08% w/v AuNP film would be > $200 – an estimate that does not consider labor or energy expenses. Thus, despite the excellent efficiency of AuNPs, they are not cheap enough to be a general alternative heat source to current synthetic methods, and investigating less expensive materials becomes important.

Another issue with AuNPs is their stability. The mass loss of PPC films in Chapter **2** were not the only changes that we noted. Figure **2-1a** shows one of these films before and after irradiation. Exposure to the laser resulted in significant visible changes to the film, specifically, loss of polymer material and a change in color (brown to red). The change in color is indicative of an increase in the size of the nanoparticles from 2 to ca. 15 nm. TEM images of the films before and after irradiation (Figure **4-1**) confirm that the nanoparticles aggregated and increased in size during exposure to the laser. The change in particle size can be attributed to the relatively weak Au–Au and Au–S bonds, which allow AuNPs to undergo Coulombic explosion and melting at high temperatures.[10-15]

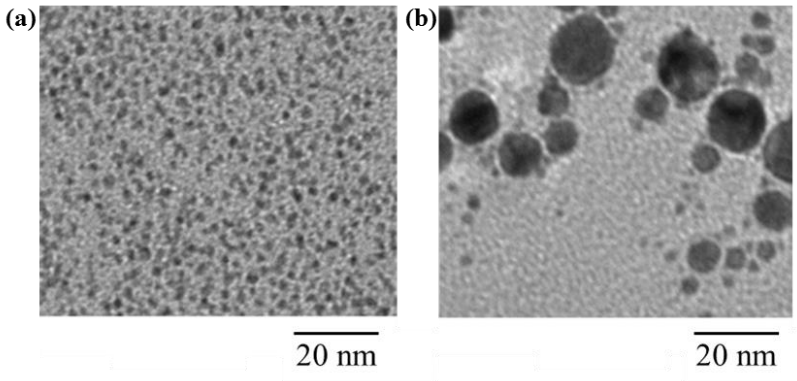

Figure **4-1**.TEM of the PPC films containing AuNPs (a) before and (b) after irradiation.[2]

The stability of a particle is critical to maintaining control over photothermal heating. Size change, which can be observed in a UV-Vis spectrum as a shift the SPR, alters the particle's ability to absorb light. A change in particle size also alters the diffusion of thermal energy to its surroundings. While small particles dissipate heat quickly, larger particles take much longer due to their increased thermal mass and radius of diffusion.[16] Altering heat delivery time over the course of a reaction reduces our ability to control the distribution of this heat within a sample. Specificity relies upon consistent heat delivery during a reaction; therefore, changing the size and thus the ability of a particle to convert light to heat is undesirable. In addition to σ_{abs} and diffusion time, the size of particles also controls the heat capacity of the particles, altering the amount of thermal energy each particle will diffuse into the surroundings. Consequently, while AuNPs do not photobleach, their poor stability in shape and size changes the ultimate temperature and temperature decay rates near the particle, also affecting control. Therefore, a good photothermal agent must exhibit stability at high temperatures.

Metal Oxide Nanoparticles

Metal oxide nanoparticles can be produced in an extensive variety of compositions and geometries that can exhibit diverse electronic structures.[17] Fine control over their synthetic properties has allowed for their use in catalysis, sensors, optoelectronic materials, and environmental remediation.[18-20] Synthetic techniques also extend control over absorption properties, which when combined with the abundant and affordable materials that many metal oxides are composed of, make metal oxide nanoparticles good photothermal candidates.

We examined magnetite (Fe_3O_4) nanoparticles (MNPs). These particles are inexpensive to produce, magnetic, and strongly absorbing in the visible region of the electromagnetic spectrum.[21,22] In order to examine MNPs capacity as a photothermal agent, we performed the same experiment PPC decomposition presented in Chapter **2**.[22] Briefly, we incorporated MNPs

into PPC films at various mass ratios and irradiated the films with a frequency-doubled Nd:YAG laser (532 nm), and we followed polymer degradation by measuring the mass loss of the films. More detailed descriptions of experimental procedures can be found in the Appendix. We observed significant mass loss, and estimate that temperatures of at least 770 K were generated in order to account for the mass loss observed (see Appendix for calculation details). We also observe a linear relationship between MNP concentration and mass loss (Figure **4-2**). Despite the fact that MNPs absorb ~70x less light at 532 nm than AuNPs, MNPs are only 30% less efficient at thermally decomposing PPC (Table **4-1**), encouraging us to further explore alternatives to AuNPs.

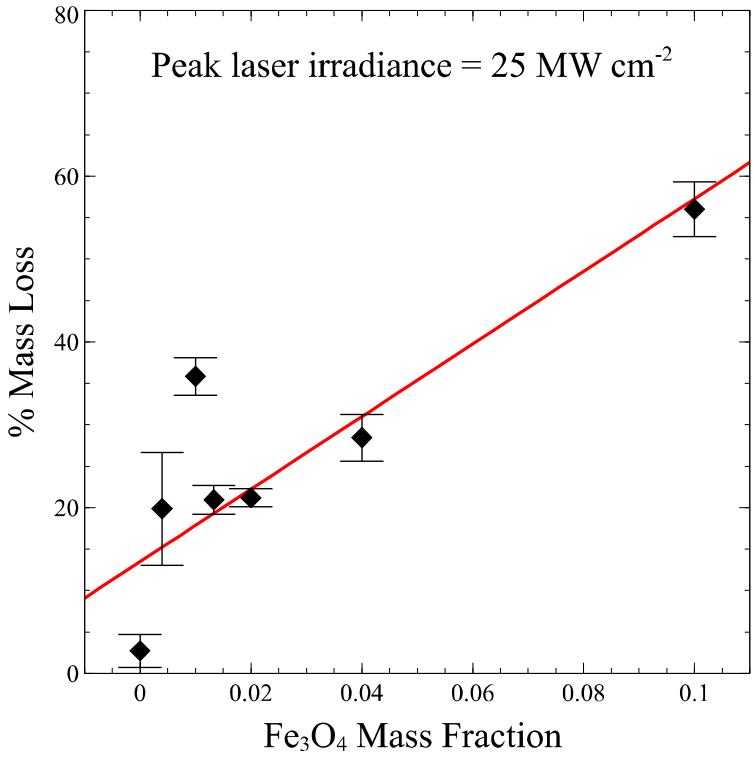

Figure **4-2** PPC films containing MNPs were irradiated and their % mass loss was plotted vs concentration of MNPs.[22]

Table **4-1**. Comparison of % mass loss imparted by irradiated PPC films containing either MNPs or AuNPs.[2,22]

X	***Mass Ratio (X:PPC)***	***% Decomposition***
MNP	1:10	56 ± 3
	1:100	36 ± 2
AuNP	1:10	72 ± 5
	1:100	82 ± 4
PPC	—	3 ± 1

After establishing that MNPs are able to efficiently absorb and convert light into heat, we examined the stability of these particles. TEM images of MNPs before and after irradiation (Figure **4-3a**) show that there is a negligible change in particle size, despite reaching high temperatures. In addition to this geometric stability, MNPs also exhibit crystalline stability. It is possible for Fe_3O_4 to become γ-Fe_2O_3 under intense heat (> 240°C), but X-ray diffraction (XRD) of the particles before and after irradiation shows that the crystal structure of the particles remains unchanged (Figure **4-3b**).[23] The crystalline and geometric stability of MNPs is due to the strong covalent attachment between MNPs and their stabilizing surfactants (oleylamine), present before and after irradiation (Figure **4-3c**). The thermal robustness of these particles coupled with their magnetic properties and efficient heat production make MNPs promising, reusable photothermal agents.

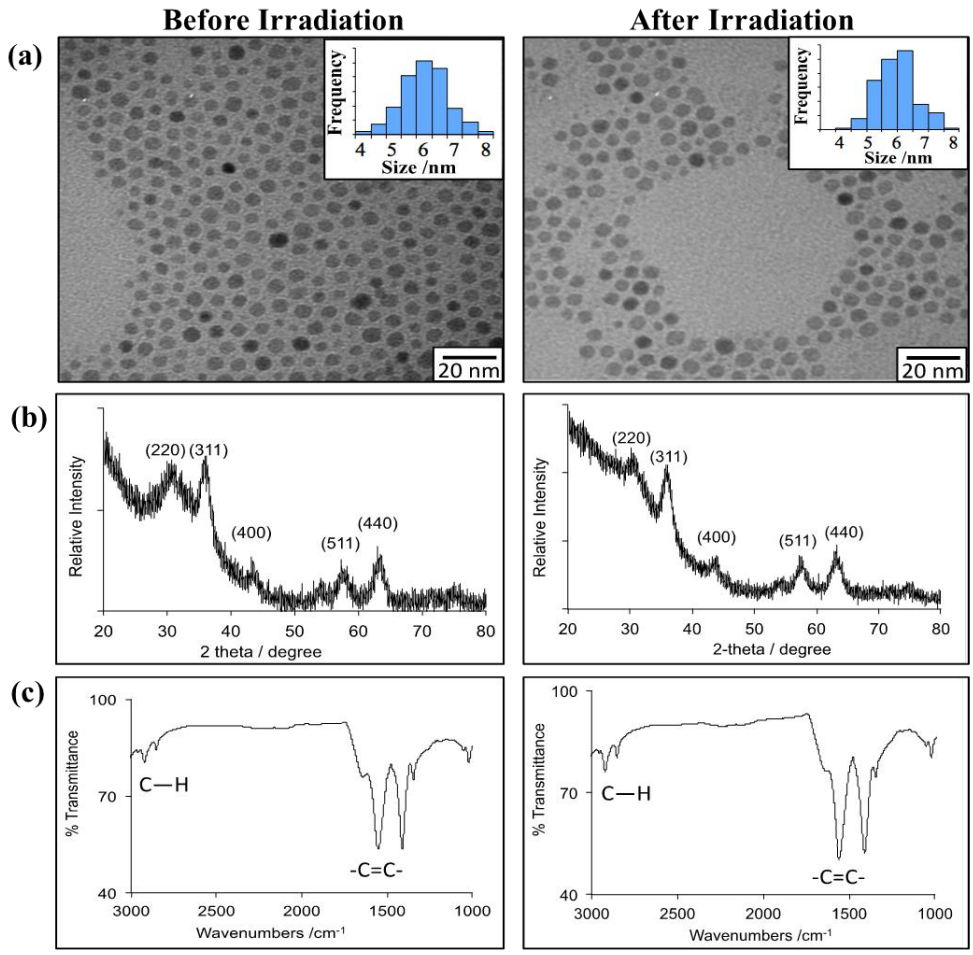

Figure **4-3**. (a) TEM images, (b) XRD, and (c) IR spectra of MNPs before and after irradiation.[22]

Unfortunately, MNPs possess some shortcomings of their own. In particular, the surface and absorption of these particles are not easily modified. Modification via ligand exchange is limited due to the strong interaction that exists between MNPs and oleylamine. Some work has been done to directly synthesize a mixed layer of oleylamine with polyethylene glycol (PEG) chains; however, in doing so, the thermal mass of these particles significantly increases and decreases the ability of heat to effect change on the environment.[24] These obstacles in surfactant modification translate to difficulties in incorporation into various solutions and substrates as well as poor efficiency in heat transfer. These nanoparticles are also only capable of absorbing visible

light, limiting the number of applications of MNPs as photothermal agents. These characteristics and limitations are shared by other metal oxides, such as PbO and Cu_2O.[25,26]

Thus far, we have examined a sampling of possible photothermal agents. However, there are many other light absorbing materials that show potential as photothermal agents. Below, we propose various light absorbing materials that may be worth investigation in the future.

Agents for the Future

Other Noble Metal Nanoparticles

The same properties that make AuNPs good light-to-heat converters apply to other noble metals, such as silver and copper. These particles are highly absorptive, easily tuned and modified, and efficiently deliver heat to the surroundings. There are also some differences between nanoparticles composed of different metals. Silver nanoparticles (AgNPs) and copper nanoparticles (CuNPs) can absorb light at higher energies than AuNPs, which means they have the potential to provide greater heating per photon.[27,28] They also exhibit antimicrobial properties and are often incorporated into medical and consumer materials such as antiseptic sprays and bandages.[29,30] The photothermal effect of these particles has been effectively utilized in cancer therapy, lithography patterning, and drug delivery.[31-33] However, these nanoparticles exhibit some drawbacks. Silver is considered toxic in biological applications, both are easily oxidized, and like gold, they are expensive materials. Furthermore, their low thermal stability and tendency to aggregate make these nanoparticles difficult to work with at photothermal temperatures.[34]

Semiconductor Nanoparticles

Similar to metal oxide nanoparticles, semiconductor nanoparticles are available in an extensive variety of combinations, which has been afforded by advancement in their synthetic techniques. Fine control over crystal structure, composition, shape, and size has opened the door to particles that can offer a wide range of properties for application in areas such as catalysis, energy storage, electronics, and optics.[35,36] These nanoparticles absorb high energy light in UV region of electromagnetic spectrum, and exhibit high photostability compared to organic dyes. While semiconductor nanoparticles are often utilized for their emissive properties, they can also convert absorbed light into heat. Theses nanoparticles possess surface defects that act as non-radiative recombination sites for excited electrons. These excited charges are trapped by the defects, which then rapidly thermalize the absorbed energy.[37] The photothermal ability of semiconductor nanoparticles, such as CuS, have been utilized in the thermal ablation of cancer cells, and are significantly less expensive than comparable AuNPs.[38] However, heat generation in semiconductors is much weaker than metallic nanoparticles, because heat dissipation occurs through interband absorption, which only allows the formation of one exciton versus the collective excitation of the surface plasmon in noble metals.[39] Therefore, large quantities of these nanoparticles would be necessary to impart significant heat.

Organic Nanoparticles

Organic nanoparticles are solid particles that are often composed of organic compounds such as lipids or polymers. Polymer organic nanoparticles are of particular interest because they are often conjugated which can lead to light absorption.[40] This conjugation also offers conductive properties that may be desirable for applications such as solar cells, sensors and photovoltaics.[41-43] When compared with organic dyes, these nanoparticles possess large absorption cross-sections

comparable to that of metallic nanoparticles, which may serve to overcome the issue organic dyes have imparting significant heat to the surroundings.40 These particles also offer a biodegradable option over their inorganic counterparts.[44] Like many of the other photothermal candidates, organic nanoparticles, such as those based on polyaniline, have been investigated for their ability to thermally ablate cancer cells.[45] However, like their smaller counter parts, organic dyes, these particles will eventually photobleach. Their light absorption is also often limited to NIR region, which results in lower energy production.[46]

Conclusions

Considering the properties listed above, we are able determine the characteristics of a good photothermal agent: strong absorption, low luminescence, effective heat delivery to the surroundings, morphological stability, and stability of surface chemistry. While facile synthesis, modification, and low cost are not requirements of a photothermal agent, they are important to consider when looking for alternatives to current heating methods as well as beneficial to implementation in a variety of applications.

Thus far, we have explored metal particles (Au), metal oxide particles (Fe_3O_4), and organic pigments (Sudan IV) as photothermal agents. It is evident that organic pigments are not capable of delivering sufficient heat to the surroundings; however, both metallic and metal oxide particles possess valuable attributes. While AuNPs are capable of delivering intense heat at various wavelengths, MNPs offer stability and low cost. Other photothermal candidates worth exploring include other strong light absorbers, such as semiconductor and organic polymers nanoparticles. These materials offer access to a wide range of absorptions and functionalities, which will allow heat to be tailored to a particular reaction or application. When combined with the localized and intense nature of this heat, this method gains further control over delivering on-demand, well-controlled heat to a wide variety of reactions and applications.

References

1. Jiang, R., Cheng, S., Shao, L., Ruan, Q. & Wang, J. Mass-Based Photothermal Comparison Among Gold Nanocrystals, PbS Nanocrystals, Organic Dyes, and Carbon Black. *J. Phys. Chem. C* **117**, 8909-8915 (2013).
2. Haas, K. M.; Lear, B. J. Degradation of polypropylene carbonate through plasmonic heating. *Nanoscale* **5**, 5247-5251 (2013).
3. Zollinger, H. *Color Chemistry: Synthesis, Properties and Applications of Organic Dyes and Pigments, 2rd Ed.* (Weinheim, VCH, 1991).
4. Ming, T., Chen, H., Jiang, R., Li, Q. & Wang, J. Plasmon-Controlled Fluorescence: Beyond the Intensity Enhancement. *J. Phys. Chem. Lett.* **3**, 191-202 (2012).
5. Link, S. & El-sayed, M. A. Shape and size dependence of radiative , non-radiative and photothermal properties of gold nanocrystals. *Int. Rev. Phys. Chem.* **19**, 409-453 (2000).
6. Nedyalkov, N. N.; Imamova, S. E.; Atanasov, P. A.; Toshkova, R. A.; Gardeva, E. G.; Yossifova, L. S.; Alexandrov, M. T.; Obara, M. Applied Surface Science 2011, 257, 5456.
7. Strong, L. E. & West, J. L. Thermally responsive polymer-nanoparticle composites for biomedical applications. *WIREs Nanomed. Nanobiotechnol.* **3**, 307-17 (2011).
8. Scaiano, J. C. & Stamplecoskie, K. Can Surface Plasmon Fields Provide a New Way to Photosensitize Organic Photoreactions? From Designer Nanoparticles to Custom Applications. *J. Phys. Chem. Lett.* **4**, 1177-1187 (2013).
9. Palesko, C.A. & Vardaman, E.J. Cost Comparison for Flip Chip, Gold Wire Bond, and Copper Wire Bond Packaging. Electronic Components and Technology Conference (ECTC), 2010 Proceedings 60th, 10-13.
10. P. V. Kamat, M. Flumiani & G. V. Hartland. Picosecond Dynamics of Silver Nanoclusters. Photoejection of Electrons and Fragmentation. *J. Phys. Chem.* **102**, 3123–3128 (1998).
11. Link, S., Burda, C., Nikoobakht, B. & El-Sayed, M. Laser Photothermal Melting and Fragmentation of Gold Nanorods: Energy and Laser Pulse-Width Dependence. *J. Phys. Chem. A* **103**, 1165–1170 (1999).
12. Link, S.; Burda, C.; Nikoobakht, B. and El-Sayed, M. How long does it take to melt a gold nanorod?: A femtosecond pump–probe absorption spectroscopic study. *Chem. Phys. Lett.* **315**, 12–18 (1999).
13. Inasawa, S.; Sugiyama, M. & Yamaguchi, Y. Laser-Induced Shape Transformation of Gold Nanoparticles below the Melting Point: The Effect of Surface Melting. *J. Phys. Chem. B* **109**, 3104–3111 (2005).
14. Hleb, E.Y. &Lapotko, D.O. Photothermal properties of gold nanoparticles under exposure to high optical energies. *Nanotechnology* **19**, 355702 (2008).
15. Pakiari, A. H. & Jamshidi, Z. Nature and Strength of M−S Bonds (M = Au, Ag, and Cu) in Binary Alloy Gold Clusters. *J. Phys. Chem. A* **114**, 9212-9221 (2010).
16. Hu, M. & Hartland, G. V. Heat Dissipation for Au Particles in Aqueous Solution : Relaxation Time versus Size. *J. Phys. Chem. B* **106**, 7029-7033 (2002).
17. Wyckoff, R.W.G. *Crystal Structures 2nd Ed.* (Wiley, New York, 1964).
18. Hoffmann, M. R.; Martin, S. T.; Choi, W. & Bahnemann, D. W. Environmental Applications of Semiconductor Photocatalysis. *Chem. Rev.* **95**, 69-96 (1995).
19. P.V. Kamat. Photochemistry on nonreactive and reactive (semiconductor) surfaces. *Chem. Rev.* **93**, 267-300 (1993).
20. Livage, J.; Henry, M. & Sanchez, C. Sol-gel chemistry of transition metal oxides. *Prog. Solid State Chem.* **18**, 259-341 (1988).
21. Sun, S.; Sun, S.; Zeng, H.; Robinson, D.B.; Raoux, S.; Rice, P.M.; Wang, S.X. & Li, G.

Monodisperse MFe_2O_4 (M = Fe, Co, Mn) Nanoparticles. *J. Am. Chem. Soc.* **126**, 273-279 (2004).
22. Johnson, R. J. G., Haas, K. M. & Lear, B. J. Fe_3O_4 Nanoparticles as Robust Photothermal Agents for Driving High Barrier Reactions under Ambient Conditions. *Chem. Commun.* **51**, 417-420 (2014).
23. Shebanova, O. N. & Lazor, P. Raman study of magnetite (Fe3O4): laser-induced thermal effects and oxidation. *J. Raman Spectrosc.* **34**, 845-852 (2003).
24. Mukhopadhyay, A., Joshi, N., Chattopadhyay, K. & de Goutam. A Facile Synthesis of PEG-Coated Magnetite (Fe O) Nanoparticles and Their Prevention of the Reduction of Cytochrome C. *ACS Appl. Mater. Interfaces* **4**, 142-149 (2012).
25. Suzuki, K.; Tanaka, N.; Ando, A. & Takagi, H. Optical Properties and Fabrication of Cuprous Oxide Nanoparticles by Microemulsion Method. *J. Am. Ceram. Soc.* **94**, 2379-2385 (2011).
26. Yousefi, R.; Zak, A.K. Jamali-Sheini, F.; Huang, N.M.; Basirun, W.J. & Sookhakian, M. Synthesis and characterization of single crystal PbO nanoparticles in a gelatin medium. *Ceram. Int.* **40**, 11699-11703 (2014).
27. Maity, S., Downen, L. N., Bochinski, J. R. & Clarke, L. I. Embedded metal nanoparticles as localized heat sources: An alternative processing approach for complex polymeric materials. *Polymer* **52**, 1674-1685 (2011).
28. Lee, K-S. & El-Sayed, M.A. Gold and Silver Nanoparticles in Sensing and Imaging: Sensitivity of Plasmon Response to Size, Shape, and Metal Composition. *J. Phys. Chem. B* **110**, 19220–19225 (2006).
29. Yamada, M., Foote, M. & Prow, T. W. Therapeutic gold, silver, and platinum nanoparticles. *WIREs Nanomed. Nanobiotechnol.* **7**, 428-445 (2015).
30. Chatterjee, A., Chakraborty, R. & Basu, T. Mechanism of antibacterial activity of copper nanoparticles. Nanotechnology **24**, 135101 (2014).
31. Kleinauskas A, Rocha S, Sahu S, Sun YP, Juzenas P. Carbon-core silver-shell nanodots as sensitizers for phototherapy and radiotherapy. *Nanotechnology* **24**:325103 (2013).
32. Kim, W. J.; Vidal, X.; Baev, A.; Jee, H. S.; Swihart, M. T. & Prasad P. N. Photothermal-reaction-assisted two-photon lithography of silver nanocrystals capped with thermally cleavable ligands. *Appl. Phys. Lett.* **98**, 133110 (2011).
33. Ramadan, S., Guo, L., Li, Y., Yan, B. & Lu, W. Hollow Copper Sulfide Nanoparticle-Mediated Transdermal Drug Delivery. *Small* **8**, 3143-3150 (2012).
34. Sun, J.; Ma, D.; Zhang, H.; Liu, X.; Han, X.; Bao, X.; Weinberg, G.; Pfander, N. & Su, Dangsheng. Toward Monodispersed Silver Nanoparticles with Unusual Thermal Stability. *J. Am. Chem. Soc.* **49**, 15756-15764 (2006).
35. O'Brien, P. *Nanoscience Volume 1: Nanostructures through Chemistry*. (The Royal Society of Chemistry, Cambridge, 2013).
36. Bangal, M.; Ashtaputre, S.; Marathe, S.; Ethiraj, A.; Hebalkar, N.; Gosavi, S. W.; Urban, J. & Kulkarni, S. K. Semiconductor Nanoparticles. *Hyperfine Interactions*. **160**, 81-94 (2005).
37. Tsuzuki, T. *Nanotechnology Commercialization* (Hoboken, Pan Stanford, 2013).
38. Li, Y.; Lu, W.; Huang, Q.; Huang, M.; Li, C. & Chen, W. Cupper sulfide nanoparticles for photothermal ablation of tumor cells. *Nanomedicine*, **5**, 1161-1171 (2010).
39. Govorov, A. O. & Richardson, H. H. Generating heat with metal nanoparticles. *Nano Today* **2**, 30-38 (2007).
40. Pecher, J. & Mecking, S. Nanoparticles of Conjugated Polymers. *Chem. Rev*. **110**, 6260–6279 (2010).
41. Gunes, S.; Neugebauer, H. & Sariciftci, N. S. Conjugated Polymer-Based Organic Solar Cells. *Chem. Rev.***107**,1324–1338 (2007).

42. Chen, J. & Cao, Y. Development of Novel Conjugated Donor Polymers for High-Efficiency Bulk-Heterojunction Photovoltaic Devices. *Acc. Chem. Res.* **42**, 1709-1718 (2009).
43. Thomas, S. W., III; Joly, G. D. & Swager, T. M. Chemical sensors based on amplifying fluorescent conjugated polymers. *Chem. Rev.* **107**, 1339-1386 (2007).
44. Lewinski, N.; Colvin, V.; Drezek, R. Cytotoxicity of nanoparticles. *Small* **4**, 26–49 (2008).
45. Yang, J.; Choi, J.; Bang, D.; Kim, E.; Lim, E. K.; Park, H.; Suh, J. S.; Lee, K.; Yoo, K. H.; Kim, E. K.; Huh, Y. M. & Haam, S. Convertible Organic Nanoparticles for Near-Infrared Photothermal Ablation of Cancer Cells. *Angew. Chem., Int. Ed*. **50**, 441-444 (2011).
46. Larson, D. R.; Zipfel, W. R.; Williams, R. M.; Clark, S. W.; Bruchez, M. P.; Wise F. W. & Webb, W. W. Water-soluble quantum dots for multiphoton fluorescence imaging in vivo. *Science* **300**, 1434-1437 (2003).

Chapter 5

Towards Establishing the Photothermal Effect as an Alternative Heat Source

The work in this dissertation was motivated by a desire to understand the applicability of the photothermal effect for driving chemical reactions. This desire, in turn, stems from the need to exert greater control over application of heat – a need common to a wide variety of disciplines, from medicine to materials to agriculture. The ultimate goal of this dissertation is to comprehensively understand the limits of photothermal heat a so that we can establish the photothermal effect as an efficient, well-controlled, and on-demand heat source.

The utility of the photothermal effect of nanoscale materials is a relatively new discovery, yet it has gained increasing interest as a molecular-scale heat source. Of particular note is the use of AuNPs to thermally ablate cancer cells. Photothermal cancer therapy relies on the delivery of intense heat to a localized region around the nanoparticles that leaves nearby healthy cells unharmed. Without an understanding of the temperatures achieved by irradiated nanoparticles, this heating technique lacks control, and in the case of cancer therapy, this lack of control could be dangerous. While many applications of the photothermal effect are not biological, this particular application demonstrates the paramount importance of understanding this heat so that it may be applied in a well-controlled manner. For higher temperature applications, understanding of how to control heat becomes more important.

My dissertation represents the first steps towards developing the photothermal effect as a well-controlled alternative heat source by exploring the kinetics of various photothermally-driven transformations (i.e. formation and cleavage of bonds). We explored several light absorbing materials so as to gain a better understanding of the characteristics and properties of a good photothermal agent. The work that we have accomplished in demonstrating the ability of the

photothermal effect of different light absorbing materials in various reaction environments is summarized below.

Using Bond Cleavage to Establish Photothermal Temperatures

Because previous work utilizing the photothermal effect has often exploited the intense heat delivered by this effect to break bonds, my work began by following the kinetics of a bond cleavage reaction. While it was no surprise that photothermal heat was capable of cleaving these bonds, this work represented the first use of photothermal heat in the solid state and the first photothermal cleavage along a known reaction mechanism. This enabled kinetic analysis, and the kinetic information we were able to extract from characterizing the product was valuable in determining the temperatures that we are capable of achieving under the photothermal effect.

Poly(propylene carbonate) (PPC) provided an ideal model system for a number of reasons. The decomposition of this polymer generated a volatile monomer, which allowed us to easily follow the extent of this reaction via mass loss. Additionally, PPC does not absorb light at the irradiation wavelength of 532 nm, ensuring that any light-to-heat conversion could be attributed to AuNPs. Finally, the combination of the first-order nature of this thermal decomposition and the well-established thermodynamic and kinetic parameters allowed us to experimentally and theoretically determine photothermal temperatures.

During this experiment, we observed a dependence on the nanoparticle concentration and found that light-to-heat conversion followed Beer's Law. Irradiated films exhibited greater mass loss in the presence of higher AuNP concentrations. However, we observed a light-limited regime, in which further AuNP concentration increases did not affect mass loss. This observation was attributed to the simultaneous increase of heat sources and a diminishing volume of film exposed to light.

With the product of decomposition verified via ^{1}H NMR, we were able to predict the temperatures achieved via photothermal heat by examining the first-order kinetics of this reaction. Experimental calculations considered the period of irradiation, mass loss of the film, and the bond broken during decomposition (C-O), and predicted that a minimum of 800 K must have been achieved throughout the film. However, the localized nature of photothermal heat leads us to believe that much higher temperatures are achieved at the nanoparticle's surface. When we considered the absorption cross section (σ_{abs}), the intensity of incident light, and laser pulse width, we found temperatures in excess of gold's boiling point (3154 K). While it is unlikely that this temperature is experimentally reached, we believe that these two temperatures provide a minimum and maximum for driving PPC decomposition using the photothermal effect.

This work shows that not only is the photothermal effect capable of efficiently driving high barrier reactions in the solid state, but that by varying the nanoparticle concentration or laser power, we can control the heat delivered to a reaction. Understanding the temperatures that can be achieved by the photothermal effect is invaluable to its development as an alternative heat source.

Constructively Using the Photothermal Effect

Current heating methods are utilized in a wide variety of fields to accomplish both bond cleavage and formation. Until now, the photothermal effect has been primarily used to cleave bonds – for example in cancer cell ablation, polymer decomposition, and drug molecule release. In order to verify the general utility of the heat, it becomes important to not only demonstrate the destructive nature of the photothermal effect, but also its constructive nature. Furthermore, driving bond formation reactions with greater efficiency than current heating methods begins to establish the photothermal effect as a viable heating method.

In Chapter **3**, we approached this problem by examining the polymerization of a urethane film as a model system. Urethane bonds between isocyanates and alcohols spontaneously form at room temperature, which provided a baseline formation rate to which we compared all other formations. However, urethane formation at high temperatures, such as the photothermal temperatures determined in Chapter **2**, was less likely to occur because the urethane bond is fairly weak (100-130 kJ/mol) and can be cleaved at elevated temperatures.[1] Additionally, the equilibrium constant at high temperatures favors the reactants. Therefore, any observed urethane bond formation can be attributed to trapping products in chemical bond's energy well during the rapid cooling.

We examined urethane polymerization under various conditions: in the presence of AuNPs, a catalyst, or both and with or without light. Polymerization rates under these conditions were then compared to the baseline polymerization rate at room temperature, in the dark. We found that polymerization rate only increased in the presence of a catalyst or in the presence of irradiated AuNPs. While a catalyst is often used in industry to increase the rate of this reaction, we found that the rate of polymerization in the presence of irradiated AuNPs was faster on a weight-by-weight basis. Because the photothermal effect absorbs and converts light into heat within ~10 ps, we can assume that heat production only occurs during periods of exposure to the pulsed light (20 μs total).[2] Considering the rate of polymerization in this short time period, we observed a billion-fold enhancement in rate.

We also observed a synergistic interaction between AuNPs and the catalyst under irradiation. In these films, there was a dramatic increase in rate of polymerization, and this increase was greater than the sum of the two effects alone. Control experiments indicate that a bulk temperature increase of ~322 K would have to occur in order to account for the kinetics we observed; however, bulk temperature measurements indicate only a 10 K temperature increase occurred. Possible reasons for this increased polymerization rate without bulk heating may be an increased mobility of reactants at elevated temperatures, which allowed them to interact with the

catalyst. Another possible explanation may be the cleavage of isocyanate trimers, which this particular formula is known to exist as, at high temperatures. This mechanism would increase the concentration of free isocyanates available to react with the alcohols and catalyst.

It is evident that the photothermal effect of AuNPs greatly increased urethane formation rate, and that this effect is also capable of enhancing existing synthetic techniques, in addition to being applied alone. More importantly, this work demonstrates that, like current heating methods, we can apply photothermal heat to constructive transformations, such as bond formation.

The collective work of Chapters **2** and **3** shows that the photothermal effect is capable of accomplishing many of the same transformations as current synthetic heating methods. The short timescales and molecular-level precision with which these transformations are accomplished, as well as the dependence of heat production on power and nanoparticle concentration allow us to exercise fine control over on-demand heating. While our work represents the first steps towards controlling photothermal heat, future work will establish it as an excellent alternative heat source to current synthetic methods. Discussed below are some future experiments that will further aid in understanding and therefore controlling the photothermal effect.

Future Work

Bond Isomerization

The most fundamental chemical transformations (e.g. bond cleavage, formation, and isomerization) can be accomplished using heat. Thus far, the photothermal effect has been shown to effectively accomplish both bond cleavage and bond formation. In order to establish the photothermal effect as an alternative heating method, it is important that it is capable of performing all of the transformations accomplished by traditional heating methods.

Isomerization is a chemical transformation that has been utilized for applications such as molecular switches, information storage devices, medicine, and fuel production.[3] Despite identical chemical compositions, isomers possess unique properties that can be achieved with high selectivity.[4] Isomerization can be accomplished at elevated temperatures, and performing this transformation under the photothermal effect would establish this effect as a general heat source with excellent control.

The E-Z isomerization of stilbene is a reversible reaction that has been utilized in molecular switches, and would be an excellent model system for photothermal isomerization.[ref] The isomerization of this molecule from *trans* to *cis* occurs under UV light (300 nm), and can reverse back to *trans* under either UV light (280 nm) or heat (Scheme **5-1**).[5] The thermal isomerization of stilbene from its *cis* to *trans* isomer has an activation energy of ~140-155 kJ/mol, and requires temperatures in excess of 200°C, temperatures we know the photothermal effect is very capable of reaching.[6,7] This isomerization would also be facile to characterize due to the unique electron transitions displayed by the two isomers, and we could follow the reaction by monitoring the shift in absorption in the UV-Vis spectrum.

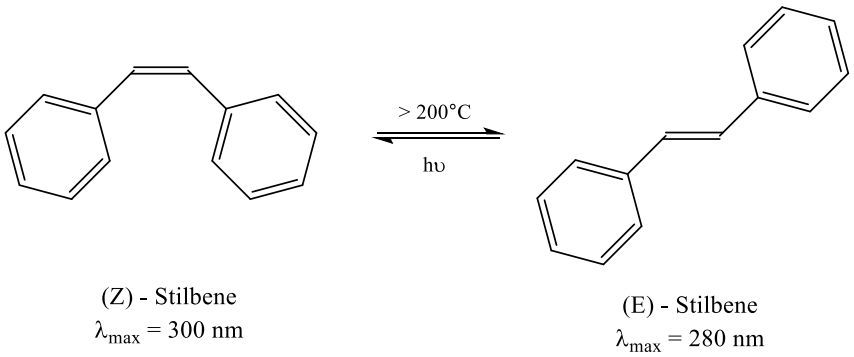

Scheme **5-1**. The reversible isomerization of stilbene from *cis* to *trans* at elevated temperatures.

The *cis* isomer can be purchased in 96% purity, and mixed neat with AuNPs or in a toluene solution. The *cis*-AuNP sample would then be irradiated with light at or near the AuNP's

λ_{max}, and away from the *cis* isomer's absorption. Photothermal heating will drive the isomerization of *cis* to *trans*, and the appearance of the *trans* isomer peak ~300 nm can be monitored using UV-Vis spectroscopy.

Reversible Reactions

Another valuable addition to the photothermal toolkit would be the ability to accomplish reversible reactions. These reactions offer access to various properties from one material, and make excellent molecular switches and self-healing materials.[8] Reversible reactions can be controlled in a number of ways, such as exposure to specific wavelengths of light or temperature. However, these stimuli are applied to bulk systems, and lack the control offered by the photothermal effect. The retro Diels-Alder (rDA) reaction is a classic example of a reversible reaction that can be thermally driven.[9] At room temperature, the equilibrium lies towards the Diels-Alder (DA) adduct, but upon exposure to elevated temperatures, the diene and dienophile are favored and a cycloreversion occurs (Scheme **5-2**).

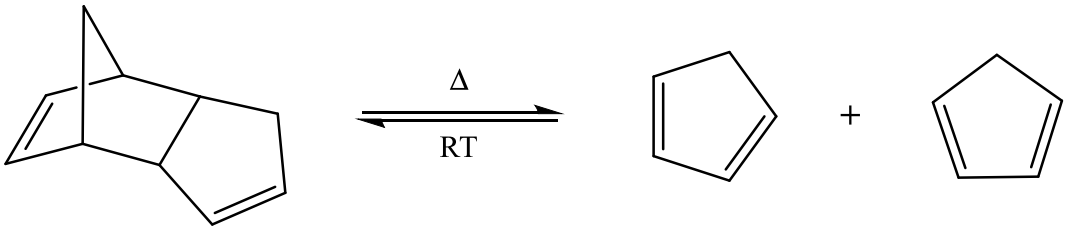

Scheme **5-2**. The retro Diels-Alder reaction results in the formation of a diene and dienophile at elevated temperatures, and will revert back to the Diels-Alder adduct at room temperature.

One possible application for this technology could be reshaping or reprocessing materials. For example, a polymer material, embedded with a photothermal agent, could be cross-linked by Diels-Alder moieties. Under irradiation, the material could be reshaped. In the

absence of light, heating will cease and the forward DA reaction will once again cross-link the polymer. This technique provides a means for altering a material after its original processing, and could be used in applications such as medical stents that may be difficult to access once implanted.

One of the limitations of this technique would be that it needs to be reversible so that the Diels-Alder adduct can spontaneously reform at room temperature. For instance, if a solid polymer generates gaseous products upon irradiation, the volatile products may evaporate and result in an irreversible reaction.

Reactions at the Nanoparticle Surface

The reactions that we have experimentally investigated thus far (PPC decomposition and polyurethane formation) were photothermally promoted by nearby AuNPs. While heat was supplied from within the reactant solution or film at the molecular level, this heat may still be considered "bulk"-level heating on a much smaller scale. The intense heat generated on the molecular level is highly localized and provides an excellent means for spatial control; however, it may also reduce the fraction of reactant molecules affected by this heat to those within several nanometers of the particle's surface. Consequently, systems may require longer heating periods, which may be detrimental to the reactive molecule or the photothermal agent (Figure **4-1**).

One solution to molecular-level "bulk" heating would be to attach a reactive molecule to the nanoparticle's surface. In the case of 2 nm AuNPs, the long alkyl chains anchored by thiol linkages, which stabilize the particle's surface, can be terminated with an alcohol or carboxylic acid, and these end groups can undergo an esterification reaction. The cleavage of an ester is a thermal process that can serve as a model system for following a photothermal reaction of an attached molecule (Figure **5-1**).

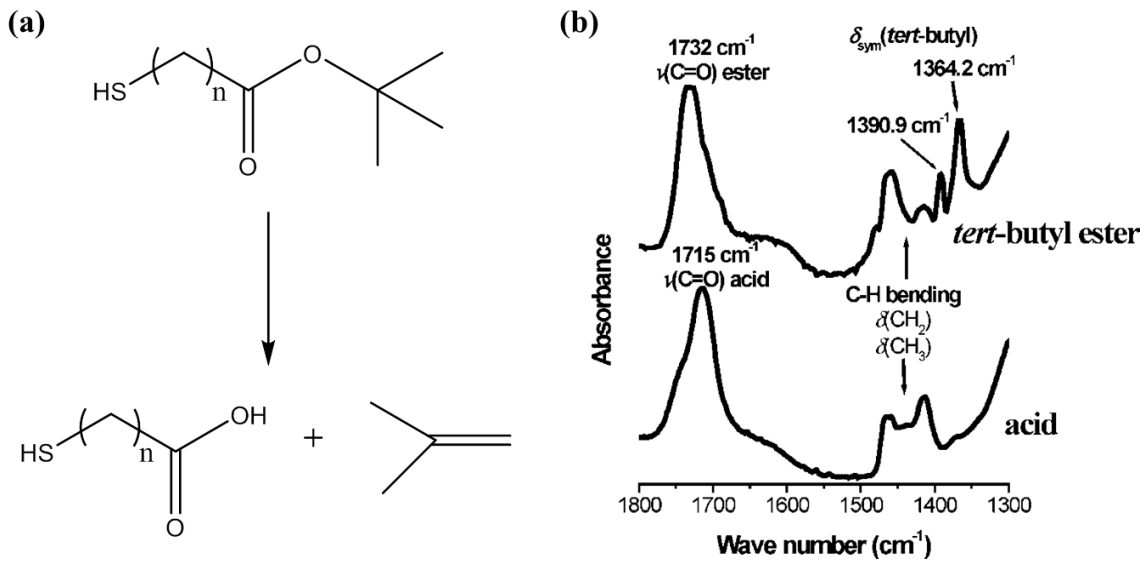

Figure **5-1**. (a) Ester cleavage can be accomplished at high temperatures, and the progress of this reaction can be monitored by (b) following changes in the IR spectrum.[10]

The reaction shown in Figure **5-1a** requires temperatures in excess of 265°C, which results in distinct changes in the C=O stretch from 1732 to 1715 cm^{-1} and the disappearance of the *tert*-butyl ester band at 1364 cm^{-1} (Figure **5-1b**).[10] The ester bond is also a good means for attaching other reactive molecules to the particle's surface by functionalizing the surface ligand and reactive moiety with complementary alcohol and carboxylic acid end groups.

In addition to driving a reaction closer to the heat source, following the progress of a reaction occurring at the particle's surface may also allow us to understand the effectiveness of dissipated heat from the particle's surface. By varying the length of the alkyl chain, we could control the distance of the reactive molecule from the particle surface, which will in turn change the heating it experiences. While it is expected that the most intense heat is experienced closest to the surface, we could determine the distance at which photothermal heat is no longer effective. In this sense, the reactive molecule would function as a molecular thermometer. Following such a reaction with time resolved spectroscopy would provide means for mapping photothermal heat both spatially and temporally.

Modification the particle's surface may alter its solubility, which may then determine the allowed degree of functionalization. Additionally, the Au-S bond is relatively weak, and high temperatures generated at the particle surface have been shown to cleave this bond (Chapter **2**). Therefore, lower irradiation fluencies or alternative linkages, such as bi- or tri-dentate thiols, may be required. The ester linkage can also be reversible at high temperatures, so if this bond is utilized as a linker and is not the thermal reaction of interest, it would be important to utilize a reaction that is thermally-triggered driven at lower temperatures than the de-esterification.[10]

Varying Pulse Repetition Rate

While the photothermal effect has been observed in systems exposed to continuous wave (CW) or pulsed light, pulsed light is often favored over CW for its ability to achieve higher temperatures (Figure **5-2**).[11] Furthermore, pulsed light also allows particles to thermally relax to ambient temperatures before absorbing and thermalizing light from the next pulse. This relaxation period between pulses allows for the complete diffusion of heat from the particle. On the other hand, particles exposed to CW light remain in a state of elevated temperature than can be detrimental to the particle's stability. These factors influenced our decision to work with pulsed light.

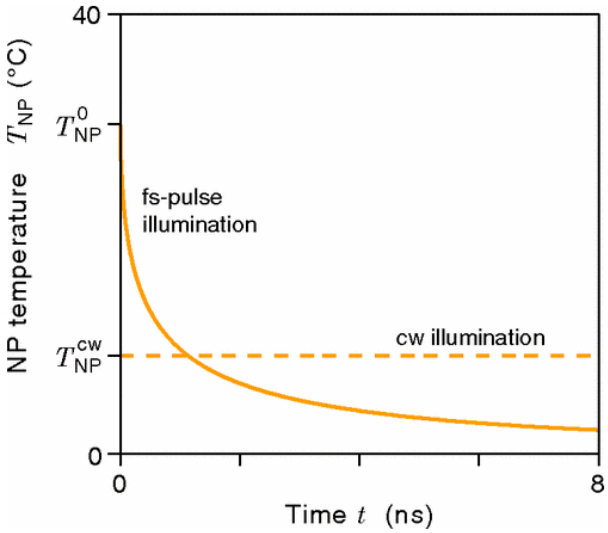

Figure **5-2**. Evolution of the temperature of a nanoparticle with r = 50 nm under pulsed light (solid line) and CW light (dashed light).[11]

The work performed in this dissertation utilized a pulsed Nd:YAG laser with a pulse width of 8 ns and a repetition rate of 10 Hz. Despite the success of our experiments, the sample is in darkness for 99.99999% of the total irradiation period. Because the production of heat relies on the absorption of light, this experimental set up is not a particularly efficient use of time.

An immediate improvement to our technique would be to increase the repetition rate of the laser's pulse. The photophysics of small nanoparticles implies that we could increase this rate by several orders of magnitude to 100 MHz (at the same pulse width) which would result in 80% of every second exposed to light, providing a 100 million times more "light time" than the 10 Hz sample experiences. It should follow then that we will observe a 100 million-fold enhancement in a photothermally-driven reaction, and that further increase in repetition rate would continue this trend. However, as mentioned above, pulsed light allows a nanoparticle to thermalize and diffuse this heat into the surroundings before the next pulse of light. When there is insufficient time between pulses to allow for thermal relaxation, the effects of pulses begin to overlap, and the particle remains in a state of elevated temperature.[11] The temperature profile of the nanoparticle then begins to resemble that expected for CW irradiation. Therefore, there must be at least a time

period of at least 10 ps between pulses in order to maintain pulse localization. For a 10 ns pulse width, a pulse frequency limit would occur at approximately 100 MHz.

Varying Pulse Width

In addition to varying pulse frequency, the pulse width may also be adjusted. Work performed by Lukianova-Hleb *et al*. examined the generation of a vapor bubble around a AuNP irradiated with light of pulse widths varying from ps to CW.[12] This work showed that while the shortest laser pulse (20 ps) generated bubbles at the surface of the particle, CW light required 9 orders of magnitude more energy to generate a bubble. This work illustrates the localized heating exhibited under pulsed irradiation versus the bulk heating observed under CW light.

The photophysical event responsible for the production of heat via the photothermal effect occurs within ~10 ps (Scheme **1-1**), and laser pulses that are longer than the thermal relaxation time of the particle will cause heating of both the particle and surrounding medium as heat diffuses away from the particle's surface.[13] Conversely, when the pulse is much shorter that thermal relaxation, then this energy is confined within the particle, resulting in rapid heating of the particle.[13] The 8 ns pulses we have utilized in our work are ~800x longer than the thermalization of a particle. During this period of time, the particle will initially deliver intense heat to the surroundings. However, over time the particle would approach a steady-state temperature with smaller temperature changes. Shorter pulse widths would maximize the initial intense heat delivery, and are desirable for delivering heat to the surroundings without altering the nanoparticle's stability. Finding the optimal pulse width is critical to efficiently using the photothermal effect.

Conclusions

My dissertation contributes to the understanding of the photothermal effect, and demonstrates molecular-level control that can be exercised with this heat. This work demonstrates the ability of photothermal heat to drive transformations fundamental to science, and establishes its potential as a well-controlled and on-demand tool. This technique can be applied to a diverse set of chemical reactions in a wide variety of disciplines. Further work on the technique will improve the efficiency and efficacy of many applications, as well as further demonstrate the breadth of its applicability.

References

1. Chattopadhyay, D. K.; Webster, D. C. Progress in Polymer Science 2009, 42, 1068.
2. Link, S. & El-Sayed, M. A. Shape and Size Dependence of Radiative , Non-Radiative and Photothermal Properties of Gold Nanocrystals. *Int. Rev. Phys. Chem.* **19**, 409-453 (2000).
3. Garcia-Amoros, J.; Sanchez-Ferrer, A.; Massad, W.A.; Nonell, S. & Velasco, D. Kinetic study of the fast thermal *cis*-to-*trans* isomerization of *para*-, *ortho*- and polyhdroxyazobenzenes. *Phys. Chem. Chem. Phys.* **12**, 13238-13242 (2010).
4. Marinetti, A.; Jullien, H. & Voituriez, A. Enantioselective, transition metal catalyzed cycloisomerizations. *Chem. Soc. Rev.* **41**, 4884-4908 (2012).
5. Reusch, W. *Virtual Textbook of Organic Chemistry* (Michigan State University, 1999).
6. G. S. Hartley "The cis form of Azobenzene" *Nature* **140**, 281 (1937).
7. Taylor, T. W. J. & Murray, A. R. Isomeric Change in Certain Stilbenes. *J. Chem. Soc.*, 2078–2086, (1938).
8. Engel, T. & Kickelbick, G. Thermoreversible Reactions on Inorganic Nanoparticle Surfaces: Diels–Alder Reactions on Sterically Crowded Surfaces. *Chem. Mater.* **25**, 149-157 (2012).
9. Rickborn, B. *The Retro–Diels–Alder Reaction Part I. C-C Dienophiles*. Organic Reactions. 52:1:1–393 (2004).
10. Dugas, V. & Chevalier, Y. Chemical reactions in dense monolayers: in situ thermal cleavage of grafted esters for preparation of solid surfaces functionalized with carboxylic acids. *Langmuir* **27**, 14188-14200 (2011).
11. Baffou, G. & Rigneault, H. Femtosecond-pulsed optical heating of gold nanoparticles. *Phys. Rev. B*, **84**, 035415 (2011).
12. Lukianova-Hleb, E. Y., Volkov, A. N. & Lapotko, D. O. Laser Pulse Duration Is Critical For the Generation of Plasmonic Nanobubbles. *Langmuir* **30**, 7425-7434 (2014).
13. Pustovalov, V. K. Theoretical study of heating of spherical nanoparticle in media by short laser pulses. *Chem. Phys.* **308**, 103-108 (2005).

Kaitlin M. Haas

Department of Chemistry, The Pennsylvania State University, 103 Chemistry Bldg., University Park, PA 16802

Education

The Pennsylvania State University — **University Park, PA**
Ph.D. Chemistry, Advisor: Benjamin Lear — August 2015
Dissertation: "Driving thermally-activated chemical reactions with molecular-scale control using the photothermal effect of nanoparticles"

St. John's University, — **Queens, NY**
B.S. Chemistry (ACS certified degree), Advisor: Elise Megehee — May 2010
Thesis: "Synthesis of Luminescent Ruthenium Complexes Containing Bipyridine and Bidentate *N*-Heterocyclic Carbene Ligands Using a Triflate Intermediate"

Research Experience

The Pennsylvania State University — **University Park, PA**
Advisor: Benjamin Lear — Fall 2010-August 2015
Investigated the photothermal properties of gold nanoparticles and the chemical availability of heat produced for use in thermally driven reactions by probing the surface plasmon on nanoparticles with a Nd:YAG laser

St. John's University — **Queens, NY**
Advisor: Dr. Elise Megehee — Fall 2009-Spring 2010
Synthesized and characterized a new class of luminescent ruthenium-centered porphyrins with ^{1}H NMR, UV-Vis, chromatography

Publications

4. "Billion-fold rate enhancement of urethane polymerization via the photothermal effect of plasmonic gold nanoparticles." **Haas, K. M.**, Lear, B.J. *Chemical Science*, **2015**, DOI: 10.1039/c5sc02149a.
3. "Fe_3O_4 Nanoparticles as Robust Photothermal Agents for Driving High Barrier Reactions under Ambient Conditions." Johnson, R. J. G.; **Haas, K. M.**, Lear, B. J. *Chemical Communications*, **2014**, *51*, 417-420. DOI: 10.1039/c4cc07966c.
2. "Science Under Extreme Conditions." **Haas, K. M**. *Focus on Materials*, **2013**, 28-30.
1. "Degradation of polypropylene carbonate through plasmonic heating." **Haas, K. M.**; Lear, B. J. *Nanoscale*, **2013**, ***5***, 5247-5251. DOI:10.1039/c3nr01498c

Selected Presentations

1. "Mapping the chemical relevance of the surface plasmon." **Haas, K. M.** & Lear, B.J. American Chemical Society National Meeting. San Francisco, CA, August 2014. *Oral Presentation*
2. "Transduction of light to heat: Driving chemical reactions *via* plasmonic heating." **Haas, K. M.** & Lear, B. J. American Chemical Society National Meeting. New Orleans, LA, April 2013. *Oral Presentation*
3. "Transduction of Light to Heat: Driving Chemical Reactions *via* Plasmonic Excitation." **Haas, K. M.** & Lear, B. J. American Chemical Society National Meeting. Philadelphia, PA, August 2012. *Poster Presentation*

Selected Honors and Awards

The Pennsylvania State University — **University Park, PA**
Penn State Continuing Graduate Research Dalalian Fellowship Award — Fall 2014-Spring 2015
Harry and Catherine Dalalian Graduate Fellowship in Organic Chemistry — February 2013
Rustum and Della Roy Innovation in Materials Research Award — January 2013
DOW Travel Award — April 2012
W. Donald Miller Graduate Fellowship — November 2011

St. John's University — **Queens, NY**
Big East Academic Honors — Fall 2008-Spring 2010
Recognizes outstanding academic performance by student athletes in the NCAA Big East Conference.

Affiliations and Extracurricular Activities

Girl Scout Workshop Chair — Fall 2013-Spring 2014
Eberly College of Science and Chemistry Dept. Climate and Diversity Committee Member — Fall 2014-Summer 2015
Graduate Women in Science at Penn State Member — Fall 2011-present
St. John's University Women's Varsity Soccer, Division I — Fall 2006-Spring 2010